Gas temperature determination from rotational lines in non-equilibrium plasmas : a review

Gas temperature determination from rotational lines in non-equilibrium plasmas: a review

2014 Plasma Sources Sci. Technol. 23 023001

IOP Publishing Plasma Sources Science and Technology

Plasma Sources Sci. Technol. **23** (2014) 023001 (32pp) doi:10.1088/0963-0252/23/2/023001

Invited Review

Gas temperature determination from rotational lines in non-equilibrium plasmas: a review

P J Bruggeman[1], N Sadeghi[2], D C Schram[3] and V Linss[4]

[1] Department of Mechanical Engineering, University of Minnesota, 111 Church Street SE, Minneapolis, MN 55455, USA
[2] LIPhy, Université de Grenoble 1/CNRS, UMR 5588, Grenoble F-38041, France
[3] Department of Applied Physics, Eindhoven University of Technology, P O Box 513, 5600 MB, The Netherlands
[4] VON ARDENNE GmbH, Plattleite 19/29, 01324 Dresden, Germany

E-mail: pbruggem@umn.edu

Received 23 September 2013, revised 8 January 2014
Accepted for publication 10 January 2014
Published 7 April 2014

Abstract

The gas temperature in non-equilibrium plasmas is often obtained from the plasma-induced emission by measuring the rotational temperature of a diatomic molecule in its excited state. This is motivated by both tradition and the availability of low budget spectrometers. However, non-thermal plasmas do not automatically guarantee that the rotational distribution in the monitored vibrational level of the diatomic molecule is in equilibrium with the translational (gas) temperature. Often non-Boltzmann rotational molecular spectra are found in non-equilibrium plasmas. The deduction of a gas temperature from these non-thermal distributions must be done with care as clearly the equilibrium between translational and rotational degrees of freedom cannot be achieved. In this contribution different methods and approaches to determine the gas temperature are evaluated and discussed. A detailed analysis of the gas temperature determination from rotational spectra is performed. The physical and chemical background of non-equilibrium rotational population distributions in molecular spectra is discussed and a large range of conditions for which non-equilibrium occurs are identified. Fitting procedures which are used to fit (non-equilibrium) rotational distributions are analyzed in detail. Lastly, recommendations concerning the conditions for which the gas temperatures can be obtained from diatomic spectra are formulated.

Keywords: optical emission spectroscopy, gas temperature, rotational temperature

(Some figures may appear in colour only in the online journal)

1. Introduction

Non-equilibrium plasmas are an active research area mainly driven by their large application potential for many different disciplines ranging from environmental, chemical (synthesis), material processing, energy and biomedical applications. These plasmas are not only interesting as tools of applications but have very distinctive physical and chemical properties which are unique and directly related to the non-equilibrium nature of the plasma. On the other hand, this non-equilibrium property can cause significant complications in the measurement of different plasma parameters such as the gas temperature. The non-equilibrium is caused by the fact that the different species (e.g. electrons, ions, neutrals, radicals) are not in equilibrium with each other and can have significantly different kinetic energies. More specifically, this means that

the translational energy of electrons (which are driven by the electric field) is typically much larger than the translational energy of the heavy neutral species. This leads to much larger electron temperature (T_e) compared with the gas temperature (T_g), which is representative of the kinetic energy of neutral particles. Apart from the non-equilibrium between different species, the different degrees of freedom (rotation, vibration, translation, electronic excitation) in a molecule can also be out of equilibrium. This leads to the often cited inequality of the corresponding temperatures: $T_{trans} \leqslant T_r \leqslant T_{vib} \leqslant T_{ex} \leqslant T_e$.

In the above description, temperatures are used to label different distributions which are not in equilibrium with each other. This immediately raises a question: what is the (physical) meaning of all these different temperatures? In the case of, e.g., the rotational temperature, it describes the Boltzmann distribution by which the different rotational states of the molecule are populated. As a temperature is defined from a definition of entropy (e.g. Boltzmann–Gibbs entropy) in thermodynamics, it means that the distribution characterized by this temperature needs to be, by definition, an equilibrium distribution. It is immediately clear that when the time required for equilibration of a rotational distribution is not significantly shorter than the inflow time of molecules into this rotational manifold, (of which the populations of the rotational states depend on the formation process) the assumption of an equilibrium Boltzmann distribution can become invalid. As the title of this review already suggests, this interesting aspect of non-equilibrium plasmas forms the basis of this review. Specifically gas temperature determination from diatomic rotational distributions in non-equilibrium plasmas will be reviewed.

The gas temperature is an important plasma parameter as it strongly influences the plasma chemistry which drives most plasma applications. In addition, many applications including the treatment of heat sensitive surfaces such as polymers and wounds require limited heat loads and thus an accurate measurement of the gas temperature or heat flux is needed.

Gas temperature measurements in non-equilibrium plasmas are indeed often obtained by emission spectroscopy from the population distribution in rotational levels of excited states of diatomic molecules (rotational temperature) and have been applied for many years with great success [1–4]. It is therefore very important to have a good foundation of this particular diagnostic. This is especially the case in view of the many non-equilibrium atmospheric pressure plasmas used for applications which are often produced in a complex mixture of several molecular species. The extensive use of rotational spectra obtained by optical emission spectroscopy in the field of non-equilibrium plasmas is motivated by both tradition and the availability of low budget spectrometers. However, as indicated above, it is not automatically guaranteed that in non-equilibrium plasmas the density distribution in the monitored rotational manifold of the diatomic molecule is in equilibrium with the translational (gas) temperature. Often, non-Boltzmann rotational distributions are found in the molecular spectra of non-equilibrium plasmas, which clearly indicate the importance of interpreting rotational spectra with care.

An example of a non-equilibrium rotational distribution of OH(A) in an atmospheric pressure discharge in a vapor bubble is shown in figure 1. In the case of a Boltzmann plot, as in figure 1, a thermalized distribution would follow a straight line, of which the slope depends on the rotational temperature. The rotational levels of OH(A) with rotational number larger than 10 are clearly more populated than would be expected from the gas temperature of 1550 K as obtained by the rotational temperature of the $N_2(C)$ state. Below, it will be shown that this is due to the formation process which more efficiently populates the high N levels of OH(A); even at atmospheric pressure collisions with the background gas are not sufficiently efficient to induce a full translation–rotational equilibrium. Consequently, only the lowest rotational levels are thermalized. The appearance of such a distorted distribution is mainly possible due to quenching collisions which significantly reduce the effective lifetime of the OH(A) state. In addition, this example shows clearly that the nature of non-equilibrium is species dependent as for the case of the $N_2(C)$ state, in good approximation a thermal distribution was found [5]. The significantly larger rotational constant of OH compared with N_2 is (partly) the reason the excited states of N_2 are thermalized. However non-equation $N_2(C)$ states have also been observed (see further). Even in significantly non-thermalized distributions, as shown in figure 1, in many cases a thermalized distribution is found for low N. This illustrates the success of the use of rotational spectra as a diagnostic for gas temperatures for decades.

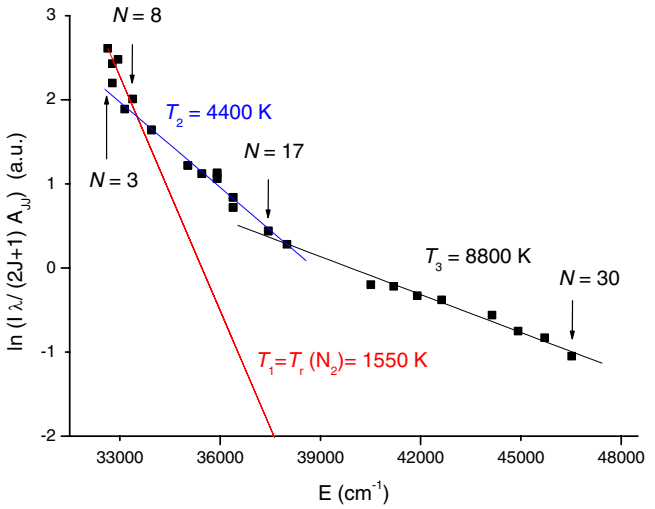

Figure 1. Boltzmann plot of the rotational distribution of OH(A) as obtained from the emission spectrum of OH(A–X) from a discharge in vapor bubble in water. The gas temperature as estimated from the rotational temperature of $N_2(C)$ is 1550 K and the corresponding expected thermal rotational population distribution is shown [5].

First, an overview of the different techniques which can be used for gas temperature determination in non-equilibrium plasmas is given. The rest of this review deals with the spectroscopy based on the emission intensity of rotational lines and is set up to provide the necessary background to answer one question: for which conditions are the rotational levels of the excited states producing the emission in translational–rotational equilibrium? To answer this question in detail, both the production mechanisms of the molecule in the excited state which determine the nascent rotational distribution and

the thermalization processes (related to the rotational energy transfer (RET)) are treated in detail. Several specific cases of commonly used transitions are discussed for different plasma conditions. The last part of this review deals with possible experimental artifacts when recording spectra, and the spectra interpretation and analysis. To conclude, the use of non-equilibrium rotational distributions, both for the gas temperature determination and the investigation of the kinetics of the excitation processes, is summarized and an outlook is given.

The review is intended as a reference guide for particular issues encountered in gas temperature measurements of non-equilibrium plasmas. It is the authors' hope that it can provide a useful overview of the topic especially for researchers involved with plasmas without a spectroscopy background but also for experienced spectroscopists. Note that most models describing plasma kinetics are only resolved up to the vibrational levels of the molecules. This review is also intended as a summary of what is known of rotational excitation and processes in plasmas from an experimental point of view.

2. Methods of gas temperature determination

In plasmas, it is often difficult to measure directly with a thermometer the accurate gas temperature. However, there are several other techniques which allow the determination of the gas temperature with good accuracy. An analysis of gas temperature measurements (and other plasma parameters) specifically for microplasmas can be found in [6]. The different techniques can be divided according to their physical principles into four categories:

(i) rotational distribution of molecules (mostly diatomic);
(ii) line profiles;
(iii) neutral density;
(iv) thermal probes.

A short overview of the above techniques used in the plasma field to obtain gas temperatures follows.

2.1. Rotational distribution of molecules

Most non-equilibrium plasmas produce significant visible and near UV emission from excited molecules. It is thus relatively easy to detect and analyze the emission with a spectrometer [1–4]. As the lifetime of the molecules in the ground state is normally significantly larger than the characteristic time between collisions, the rotational temperature of the ground state molecules is usually a good representation of the gas temperature. However, so-called active diagnostics such as laser-induced fluorescence (LIF), absorption or Raman scattering techniques are necessary to record the rotational distribution of the ground state.

Absorption signals of different rotational lines (when the line profile is known) allow determination of the absolute density in the corresponding rotational levels of the ground state ($n_{J''}$), which obey the following Boltzmann relation with rotational temperature T_{rot}:

$$n_{J''} \propto (2J''+1)\exp(-\frac{E_{J''}}{kT_{\mathrm{rot}}}), \qquad (1)$$

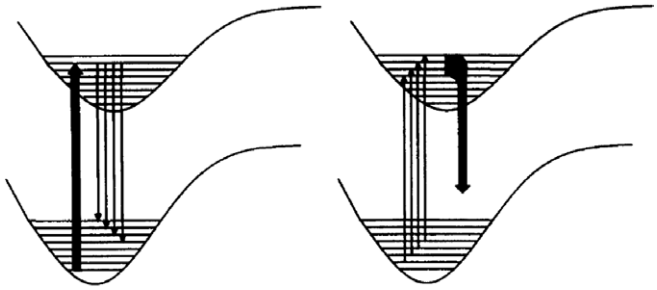

Figure 2. Schematic energy level diagrams illustrating how fluorescence (left) and excitation (right) spectra are obtained [10]. For details see text.

with $E_{J''}$ the rotational energy of the level J''. The lower state is denoted with double prime and the upper state, formed after the absorption of a photon, with single prime. The above relation allows deduction of the rotational temperature of the ground state considering that

$$\frac{I_{\mathrm{abs}}}{I_0} \propto B_{J'J''}n_{J''} \propto B_{J'J''}(2J''+1)\exp\left(-\frac{E_{J''}}{kT_{\mathrm{rot}}}\right), \qquad (2)$$

with $B_{J'J''}$ the Einstein B absorption coefficient. Examples using this technique can be found in [7–9] and with cavity ringdown in e.g. [228].

Raman scattering is the inelastic scattering of light on molecules and can also be used to obtain the rotational temperatures in the ground state of homonuclear diatomic molecules such as nitrogen or hydrogen. This has often been performed in flame studies [11, 12]. Coherent anti-Stokes Raman spectroscopy (CARS), which is a more sophisticated and highly sensitive version of the Raman spectroscopy, has recently been used to study rotation–translation equilibrium in nitrogen plasmas [13].

A third often-used technique is LIF. A laser is tuned to a molecular transition to excite it and the fluorescence of the produced excited state is detected. This technique is often applied in plasma physics and combustion [10, 14]. With LIF, depending on conditions, rotational temperatures of molecules in both ground state and excited state can be determined. A schematic representation of how the fluorescence and the excitation spectra are obtained is shown in figure 2. The so-called excitation spectra obtained from LIF can be used to obtain the ground state rotational temperature. In this case, the laser is scanned over different rotational transitions and the total fluorescence for each excitation is measured and plotted as a function of the laser wavelength. If one assumes that the fluorescence only depends on the laser excitation rate, i.e. on the ground state population and the Einstein B absorption coefficient, one can easily understand that the LIF intensities scale the same as absorption signals:

$$\int I_{J''}\mathrm{d}\lambda_{\mathrm{emis.}} \propto B_{J'J''}n_{J''}\nu_{J'J''} \propto (2J''+1)B_{J''J'}\nu_{J'J''} \times \exp\left(-\frac{E''_J}{kT''_{\mathrm{rot}}}\right), \qquad (3)$$

with $\nu_{J'J''}$ the frequency corresponding to the transition. The above assumption is not always valid (the fluorescence

intensity can be reduced by collisional quenching of the laser-excited molecules, which can be rotational level dependent) and often a complex model of the excitation and the fluorescence, including collisional processes, needs to be made (see, e.g., [10] and references therein).

Fluorescence spectra (i.e. spectrally resolved fluorescence originating from typically a single rotational transition excited by the laser at a fixed wavelength) can also be used to measure the rotational temperature of the excited state if the lifetime of the excited state is significantly longer than the time necessary for the thermalization of the rotational levels in the excited state. Indeed, in this case the nascent distribution of the excited rotational manifold, which is a single level, must be thermalized by collisions with the neutral gas in order to be able to derive a rotational temperature which reflects the gas temperature. This typically can only occur at elevated pressures (see also below for details). In this case, when assuming that the populations in rotational levels of the LIF spectrum are in Boltzmann equilibrium, the rotational temperature of the excited state obeys

$$I_{\mathrm{LIF}J',\mathrm{pump}\,J''} \propto A_{J'J''} n_{J'} \nu_{J'J''} \propto (2J'+1) A_{J'J''} \nu_{J'J''} \times \exp\left(-\frac{E'_J}{kT'_{\mathrm{rot}}}\right), \quad (4)$$

with $A_{J'J''}$ the Einstein A emission coefficient. An illustrative example of both excitation and fluorescence LIF OH spectra to perform gas temperature measurements in a nanosecond pulsed atmospheric pressure plasma can be found in [15].

The relation presented in equation (4) is also valid in most cases for optical emission spectroscopy; the only difference is that the excitation of the ground state molecules occurs by plasma processes (e.g. electron excitation, e-ion recombination, Penning ionization, etc) and not by a laser. Note that equation (4) illustrates why a Boltzmann plot such as in figure 1 plotting $\log I/(2J'+1)A_{J'J''}$ as a function of E'_J is very convenient. In the case of a Boltzmann distribution, the slope is inversely proportional to the rotational temperature.

The use of rotational quantum number N, or $J = N \pm \frac{1}{2}$ in the case of a doublet state like OH(X or A), depends on the coupling (Hunds case). For details of molecular structure and constants used in the above equations the reader is referred to the following standard textbooks and reference works [16–20].

2.2. Line profiles

Atomic (and molecular) transitions cause specific radiation at a fixed wavelength corresponding to the energy difference between the upper and lower level of the transition. In practice, the emission, or absorption transition always has some spectral width, induced by different mechanisms including the finite lifetime of the states (natural broadening), Doppler broadening, Stark broadening and van der Waals broadening or resonance broadening (pressure broadening). Stark broadening of, e.g., atomic hydrogen lines is often-used to measure the electron density in plasmas, as the electric micro-field at the position of the radiator induced by the electrons (and ions) determines the broadening. A detailed list of Stark broadening tables of hydrogen lines can be found in [21]. For many lines of other atoms and ions, the Stark broadening coefficients are listed in [22]. Doppler broadening is temperature dependent and the formula for the FWHM of a Doppler broadened Gaussian line profile is [23]

$$w_{\mathrm{D}} = 7.16 \times 10^{-7} \lambda \sqrt{\frac{T}{M}}, \quad (5)$$

where M is the molecular weight of the radiator in atomic mass units, T is the temperature in K and λ is the wavelength of the transition. Collisional broadening by a non-resonant particle or van der Waals broadening is both density and temperature dependent but resonance broadening only depends on the density. Assuming constant pressure, the temperature dependences of the FWHM of the (Lorentzian) line width induced by the van der Waals and resonance broadening are [23–25]

$$w_{\mathrm{vdW}} = A\frac{p}{T^{0.7}} \quad \text{and} \quad w_R = A\frac{p}{T}. \quad (6)$$

with A a constant depending on the radiator, collision partner and transition. For example, $A = 3.6$ for the H_β Balmer line in air for pressure in units bar, temperature in Kelvin and FWHM in nm [1]. Pressure broadening is only significant at low gas temperatures and high pressures. This is why it is most useful to obtain gas temperature from the FWHM of a Lorentzian profile of the line in atmospheric pressure plasmas [26]. Doppler broadening can be accurately used at low pressure and elevated temperatures, especially when pressure and Stark broadenings are not dominant. In high electron density plasmas, often both above-cited broadenings are superimposed on the Stark broadening and the accuracy of the method is reduced when the contribution of the line profile of two or more broadening mechanisms are significant. For example, in cold atmospheric plasmas with a large electron density (order 10^{20} m^{-3}) both van der Waals and Stark broadening of hydrogen Balmer lines are important (e.g. [27]). Also, when n_{e} is low, Stark broadening due to high E-fields present, e.g., in sheaths can increase line broadening and allow measurement of the electric field [28]. Wang *et al* have investigated the electric field distribution in the cathode sheath of an atmospheric pressure helium microplasma from the Stark splitting of H_β line [29]. Analysis of the line broadening mechanism from the line profile is a powerful technique but requires in most cases a high-resolution spectrometer to exploit the full potential of information hidden in it. In addition, narrow band diode lasers are a powerful tool to measure line broadening in absorption [30]. Before the advent of laser spectroscopy, line broadening was often studied by a Fabry–Pérot analyzer in combination with a filter.

2.3. Temperature through neutral density measurement

The most direct measurement of the neutral density can be obtained by Rayleigh scattering. Rayleigh scattering is the elastic scattering of photons on electrons bound to atoms and molecules. The Rayleigh scattering cross-section is species dependent and the scattered light is proportional to the amount of neutrals in the scatter volume. Assuming the ideal gas

law to be valid, at constant pressure, the amount of scattered light is thus inversely proportional to the gas temperature. Typically, measuring the plasma off and plasma on condition yields a proportional relation between the ratio of the Rayleigh scattering intensities ($I(R)$) and the gas temperatures if the gas composition does not change:

$$T_{\mathrm{on}} = T_{\mathrm{off}} \frac{I_{\mathrm{R,off}}}{I_{\mathrm{R,on}}}. \quad (7)$$

A review on Rayleigh scattering nicely illustrates all necessary concepts in considerable detail [31]. Recent examples of Rayleigh scattering measurements to determine the gas temperature can be found in [27, 32, 33]. Note that it is important in this case to deal with gases having large Rayleigh cross-sections (He has a significantly smaller Rayleigh cross-section in comparison with Ar, O_2 and N_2) to minimize the effect of scattering of the laser light on, e.g., nearby electrodes which yields a spurious scattering signal at the same wavelength. It is therefore advisable to use a two-dimensional detector for data acquisition to have a visual image of the Rayleigh signal. This technique is most accurate at moderate gas temperatures and at high pressures and is usually performed in non-equilibrium atmospheric pressure plasmas. Pressure build-up in strongly transient plasmas needs to be considered. In addition, one needs to be careful of dust-containing plasmas, which can generate an important Mie-scattering signal. The technique also needs to be applied with caution in strongly ionizing and dissociating plasmas as in these cases the plasma itself induces a significant change in the composition of the neutral species which can lead to a change in the Rayleigh scattering cross-sections or (local) pressure.

2.4. Thermal probes

Standard thermocouples composed of metal are used in many applications but in plasmas it is difficult to use them as they can be strongly influenced by the electromagnetic fields encountered in plasma environments. In addition, they can significantly influence the plasma properties, especially at high pressures. However, there exist thermometric devices based on fiber-optics which are insensitive to the electromagnetic field produced by the plasma and are suitable to be inserted into a plasma 'without major changes' in the plasma properties. A commercial fiber is available which is based on a change in the fluorescence wavelength with temperature of the fiber tip. Another technique is using a fiber Bragg grating instrument of which the Bragg wavelength changes with temperature [34]. The main advantage of this fiber technique is their easy calibration which facilitates the interpretation of the data with good accuracy. They are also very cost effective. On the other hand, especially for atmospheric pressure plasmas, even non-conducting fibers can significantly alter the discharge and one needs to consider that in nanosecond pulsed discharges the gas temperature can have strong gradients both in space and time. Thermal fluxes to surfaces or electrodes have been measured in low-pressure plasmas by Kersten *et al* [35].

2.5. Comparison and conclusion

From the above discussion, obtaining the gas temperature from the ground state molecular rotational distributions or scattering measurements is clearly preferable but they require (expensive) equipment that is not usually compatible with industrial applications or many laboratory setups. Optical emission spectroscopy is therefore a logical and good compromise because it is non-invasive and low budget spectrometers are available which enable all plasma labs around the world to perform this diagnostic. The only question one needs to be able to answer before the rotational temperature can be interpreted as the gas temperature is if the rotational levels of the excited state from which the emission is originated are in translational–rotational equilibrium. This is the focus of the rest of this review.

3. Translational–rotational equilibrium

As stated above, in non-equilibrium plasmas, the rotational temperature of a molecule in an electronic and vibrational state is not *a priori* equal to the gas temperature. Both the mechanisms producing the molecule in the state of interest and the collisional processes in that state determine whether translational–rotational equilibrium can exist or not.

Two conditions at which translational–rotational equilibrium (the rotational temperature equals the gas temperature) can *a priori* exist are the following:

- the nascent rotational distribution is a thermalized distribution or
- fast RETs occur, which thermalize the (nascent non-thermal) rotational distribution.

When one of these conditions is fulfilled, the density distribution in the rotational levels obeys the Boltzmann law. It is important to note that an experimentally obtained Boltzmann distribution is a necessary but not sufficient condition for translational–rotational equilibrium. Examples will be shown below.

As already mentioned above, there can be a significant difference between ground state and excited state rotational distributions. Similar to an excited state, the nascent rotational distribution in the ground state of a molecule can be produced with a strong deviation from a Boltzmann equilibrium. However, in most of the cases, the rotational distribution of the ground state will thermalize because the lifetime of the ground state is typically long enough to allow many collisions with heavy particles to occur. But if the mean free path between collisions is comparable to the vessel's dimensions, or if the ground state is a chemically active radical with a short lifetime, one has to take care of the production mechanism. Note that at very low pressures (i.e. the mean free path is of the order of one of the vessel dimensions) often both wall collisions (wall temperature) and bulk collisions (gas temperature) influence the rotational distribution [36]. This simplified picture can become more complicated when association processes occur at the surface (see further).

For excited states, which are commonly observed by optical emission spectroscopy, the situation is much more

critical due to their often very short lifetime. We first treat the traditional way of gas temperature measurements from rotational spectra which is applicable in two limits: at low pressures (without collisions during the lifetime of the excited state) and at high pressures (strongly collisional regime).

In the low-pressure limit, it can sometimes be assumed that the excited state is solely produced by electron excitations. Often the following assumptions can be made.

(i) The ground state distribution obeys a Boltzmann distribution and the rotational temperature equals the gas temperature.
(ii) The electron excitation does not depend on the rotational level (no change, or very small change of the rotational quantum number occurs).
(iii) The (effective) lifetime of the excited state is short in comparison with the RET time in the excited state.

In this case, the electron excitations will basically map the ground state rotational distribution onto the excited state rotational distribution. This is because the electron excitation cross-sections drop significantly for increasing ΔJ [37]. An example for homonuclear molecules (considering only $\Delta J = 0$) such as H_2 can be found in [4]. For heteronuclear molecules, it becomes more complex as normally both $\Delta J = 0, \pm 1$ need to be considered. An example for the BH(A–X) transition can be found in [38].

The nascent distribution is thus an almost thermal distribution. However, in this case one needs to use the rotational constant B'' of the ground state from which the molecule has been excited, or correct the temperature obtained with the rotational constant of the upper state B' by a factor B''/B'.

The necessary assumptions are often encountered in low pressure, low density ionizing plasmas with no collisions in the excited state during its lifetime. In this case, electron excitation is often also the dominant excitation mechanism. An example of a low-pressure plasma can be found in [39] for H_2, in which the impact of the production mechanisms on the rotational temperature is considered.

The other limiting case is the high collisional regime for relatively long-lived electronic states. In this case several collisions between a molecule in this state and the background gas occur during its lifetime. These collisions thermalize a potentially non-thermal nascent rotational population distribution before the emission of a photon. This means that the RET rate needs to be considerably larger than the depopulation rate $1/\tau_f$, with τ_f the effective lifetime of the excited state. This condition is clearly favored in high-pressure plasmas, although one must also consider that at high pressures the collisional quenching (depopulation of the excited state by collisions without the emission of a photon) can significantly reduce the effective lifetime of the excited state.

For both of these two limiting cases, the measured rotational population distribution is Boltzmann and the rotational temperature equals the gas temperature, provided the necessary correction for the difference in rotational constants of the excited and ground state has been made. However, the Boltzmann equilibrium cannot be reached in all other cases: i.e. when at least one production mechanism leads to a nascent rotational distribution which does not reflect the thermalized ground state rotational population AND the effective lifetime of the excited state is not long enough to cause thermalization by collisions (RET) of all rotational levels in these states.

An illustrative example is a LIF experiment in which a single rotational level is populated by laser excitation. The time-resolved measurements of the fluorescence spectrum of OH(A) in a 20 Torr, C_3H_8/O_2 flame at different time delays shown in figure 3 illustrate clearly the importance of thermalizing collisions when a strongly non-thermal nascent rotational distribution is produced.

If the rotational spectra are not recorded in one of the two above-cited limits, the production mechanisms always (at least partly) determine the rotational population distribution. This motivates why not only rotational thermalization times but also knowledge of the production processes of the excited state from which the emission is observed is important in the analysis of the rotational distribution. The production mechanisms involved in production of excited diatomic molecules and the corresponding nascent rotational distributions are presented in detail in the next section.

4. The production and corresponding nascent rotational population distribution of diatomic molecular states

This section introduces the production mechanisms of rotationally excited molecules in plasmas. An extensive literature is available treating this topic although the work is mainly performed in non-plasma-related research fields.

Apart from electronic excitation from the ground state to an excited state of a diatomic molecule, several other mechanisms in a plasma can be responsible for the production of electronically excited diatomic molecules. These processes include metastable (energy transfer) excitation, electron dissociative excitation, photo-dissociation of polyatomic molecules, electron–ion dissociative recombination, charge transfer and heavy particle excitation. Note that some of the above-mentioned mechanisms such as dissociative recombination and charge transfer are often important in recombining or high electron density plasmas (with a low electron temperature). On the other hand, electron (dissociative) excitation is often dominant in low electron density strongly ionizing plasmas (with a relatively high electron temperature). The importance of production mechanisms of an excited molecule thus strongly depends on the plasma properties and needs to be considered case by case for each plasma.

4.1. Excitation (and ionization) processes

If a laser with a narrow bandwidth (of the same order as the line width) is tuned to a molecular electronic transition, the excitation from one rotational level of the ground state leads to the overpopulation of a specific rotational level in the excited state. This is the absolute limit which can be achieved for a specific rotational excitation. As already shown in figure 3,

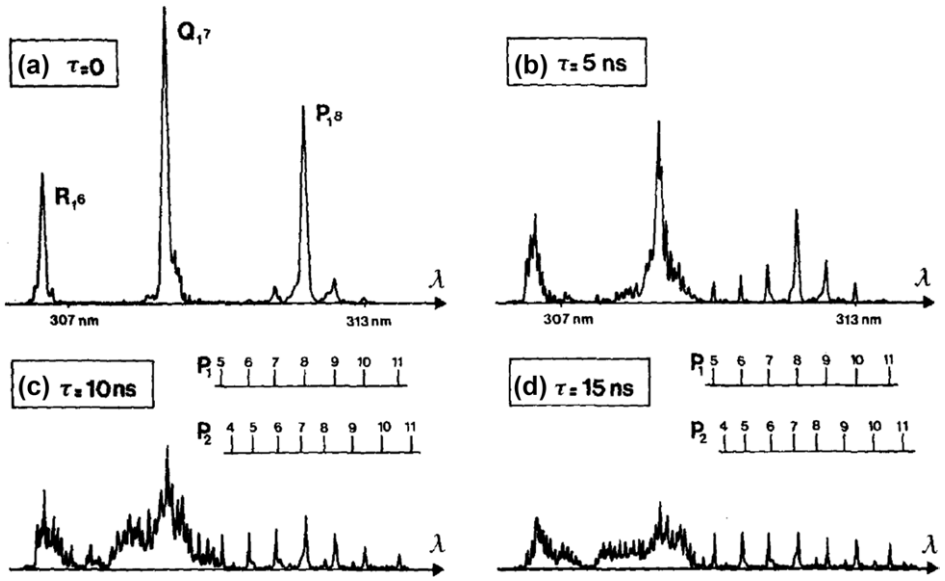

Figure 3. Fluorescence spectrum of OH(A–X) (0–0) excited by the $Q_1(7)$ (0–0) transition at delay times of 0, 5, 10 and 15 ns after the excitation. The initial fluorescence mostly originates from the $J' = 7.5$ level which is pumped by the laser. Collisional RET leads to a thermalized distribution when the delay after excitation increases [40].

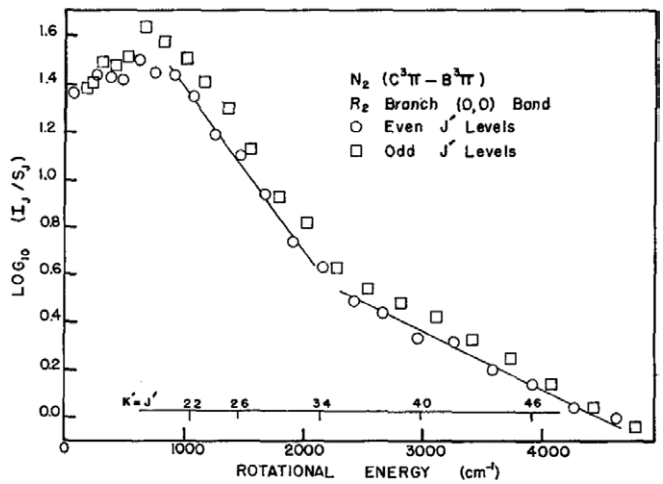

Figure 4. Rotational population distribution of $N_2(C)$ $v' = 0$ state produced by excitation of $N_2(X)$ by argon metastable atoms (predominantly in Ar ($^3P_2$) state) [41] at 1 Torr. The superposition of two linear fits corresponds to two Boltzmann distributions with temperature parameters of 950 and 2300 K, respectively.

collisional-induced rotational transfers will redistribute the single level excitation over the rotational manifold.

In the case of electron excitation from the ground state to the excited state, one can often assume that the excitation occurs without or with small change in the rotational quantum number as illustrated above (see also [37]). In the low-pressure limit (as detailed above) this leads to a rotational distribution in the excited state which is a mapping of the ground state. It will thus be a good representation of the gas temperature.

In addition, metastable excitation, charge transfer and or Penning ionization can also produce molecules in the excited states with specific rotational distributions, as illustrated in figure 4 for the excitation energy transfer from argon metastable atoms to nitrogen. The electronic energy of rare gas metastable atoms, and of some molecules such as $N_2(A)$ is indeed often high enough to electronically excite many molecules. An often encountered example in non-equilibrium plasmas is the energy transfer from argon metastable atoms in Ar($^3P_2$) and Ar($^3P_0$) states to $N_2(X)$ producing electronically excited $N_2(C)$ molecules. As this reaction is a near resonance process, it is often a dominant production mechanism in Ar discharges with small additions of N_2 or air. The density of molecules formed in rotational levels of the $N_2(C)$ state shows a specific distribution which depends not only on the electronic state of argon metastable atoms (Ar($^3P_2$) or Ar($^3P_0$)) and the bath gas temperature [42], but also on the vibrational level in which $N_2(C)$ is produced [43]. For the high rotational levels of the $v' = 0$ vibrational level of $N_2(C)$, the nascent distribution can be fitted by the superposition of two Boltzmann distributions, as shown in figure 4.

An important vibrational level dependence of the produced rotational level's density distribution has also been reported for the excitation transfer from Kr($^3P_2$) and Xe($^3P_2$) metastable atoms to nitrogen [44–48]. Energy transfer from Xe($^3P_2$) atoms selectively populates vibrational levels $v' \leqslant 5$ of the $N_2(B)$ state. Due to the possibility of collisional rotational relaxation during the rather long radiative lifetime of this state ($\tau = 4$ to $8\,\mu$s), molecular beam experiments were necessary to obtain the nascent rotational distributions [46, 47]. Despite the about $500\,\mathrm{cm}^{-1}$ endoergic character of the reaction for the $v' = 5$ level, almost 80% of the product goes to this level whose nascent rotational distribution can be represented with a rotational temperature of about 200 K, even if the ground state nitrogen molecule was at room temperature [44, 46, 47]. However, the nascent rotational temperature of the less populated lower vibrational levels $v' \leqslant 4$ can reach 3500 K [47]. Energy transfer from Kr($^3P_2$) metastable atoms also produces $N_2(B)$ molecules in vibrational levels up to $v' = 12$ [44, 48]. Under room temperature conditions, the nascent rotational distributions

correspond to rotational temperatures of about 1200 K [48]. Flowing afterglow experiments with argon and neon as carrier gas have shown [44] that the nascent rotational and vibrational distributions of $N_2(B)$ were less modified due to collisions with neon, as compared with argon as the collision partner.

Similarly, $NO(X)$ excitation by $N_2(A)$ metastable molecules has also been shown to cause large excitation of rotational levels for $N > 20$ of the produced $NO(A)$ excited state [49].

There exist examples for the excitation transfer from metastable atoms in which, due to the energy constraint (the electronic + vibrational energy of the product slightly higher than the energy of the metastable state), the rotational temperature of the nascent distribution is lower than the gas temperature. Amongst them, one can cite $N_2(B, \nu' = 5)$ produced by energy transfer from $Xe(^3P_2)$ metastable atom to N_2 [44, 46, 47] and $N_2(C, \nu' = 3)$ produced by energy transfer from $Ar(^3P_2)$ metastable atoms to N_2 [50].

An interesting case is the excitation of the $CO(X)$ molecule by $Kr(^3P_0)$ metastable atoms leading to the production of $CO(a'\,^3\Sigma^+)$ in vibrational levels $\nu' = 33$, 34 and 35 for ^{12}CO and $\nu' = 34$ to 36 for ^{13}CO [51]. In all vibrational levels, the nascent rotational distributions have been fitted with a rotational temperature of 100–150 K. If the energy constraint can be invoked for the higher vibrational levels, the production channels for $^{12}CO(a'; \nu' = 33)$ and $^{13}CO(a'; \nu' = 34)$ are exoergic by 330 cm^{-1} and 150 cm^{-1}, respectively. Surprisingly, the nascent rotational temperature in the neighboring $^{12}CO(b^3\Sigma^+, \nu' = 1)$ state, for which the excitation channel is 840 cm^{-1} endoergic, is about 300 K [51]. The first explanation proposed by the authors of [51] was the rotational angular momentum constraint during the excitation transfer reaction. The rotational constant for $CO(a'; \nu' \approx 35)$ is about 2.5 times smaller than that for $CO(X)$ [20]. If the energy transfer process occurs with approximate conservation of the rotational angular momentum of the CO molecule, since B'_v is smaller for $CO(a')$, its rotational energy is reduced. This phenomenon does not happen for $CO(b; \nu' = 1)$ which has a rotational constant close to the one of the ground state. This would definitely be a similar situation as the electron-impact excitation case of the diatomic molecule (see above) but the effect was finally attributed to the diminution of the radiative lifetime of $^{12}CO(a', \nu' = 33)$ with increasing N, which was responsible for the observed anomalous distribution in this state. Perturbation in $a'\,^3\Sigma^+$ levels ($\tau_{rad} = 3\,\mu s$) was induced by mixing of $b\,^3\Sigma^+$ state ($\tau_{rad} = 60$ ns), where mixing is increasing with N [52].

A charge-transfer reaction which is often encountered in non-equilibrium high-pressure helium plasmas is $He_2^+ + N_2 \rightarrow N_2^+(B) + 2He$. This process has been studied by Endoh *et al* [53] and exhibits high rotational excitation (figure 5). It can be approximated by a Boltzmann distribution with a temperature parameter of 900 K for $N' > 6$.

Similar results have been found for the formation of CO^+ by charge transfer from He_2^+ to CO. The rotational temperatures found by metastable induced ionization of N_2 and CO show significantly lower rotational excitation and can be approximated by Boltzmann distributions with temperature

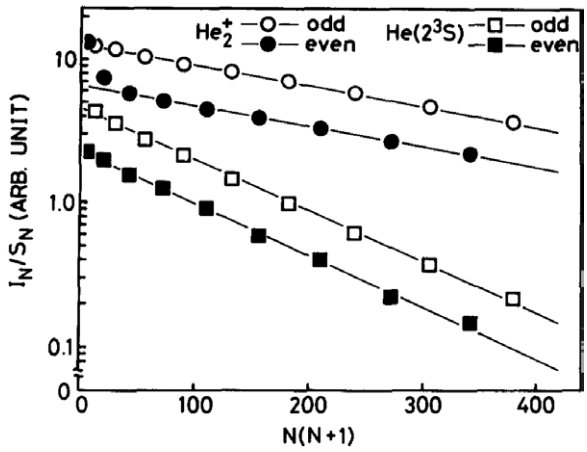

Figure 5. Rotational distributions of the $N_2^+(B)$ state produced by He_2^+-induced charge exchange and He_m Penning ionization of $N_2(X)$ [53]. The distribution corresponding to the charge exchange reaction shows high rotational excitation while the distribution corresponding to the Penning ionization is close to thermal. The temperature parameters are 900 ± 60 K and 360 ± 60 K, respectively.

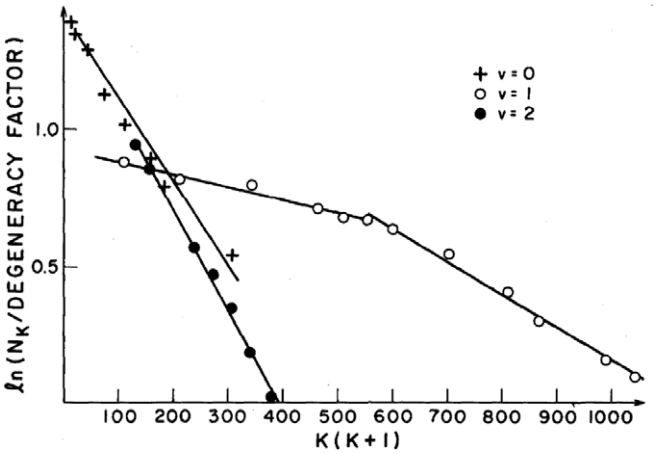

Figure 6. Nascent rotational populations of the first three vibrational levels of the $CO^+(X)$ state produced by charge exchange of N^+ with CO [54]. The rotational distributions strongly depend on the vibrational level.

parameters of 360 K and 310 K, respectively, in the case of CO [53] (see also figure 5).

Both the production of N_2^+ and CO^+ have been investigated in considerable detail for the charge transfer from Ar ions [55–57]. An interesting example is also the reaction $N^+ + CO \rightarrow CO^+ + N$. Figure 6 presents the nascent rotational populations of the first three vibrational levels of the ground state $CO(X)$ molecule, produced by charge-exchange from N^+ to CO^+ ion [54]. It is immediately clear that the rotational distributions strongly depend on the vibrational level of the exit channel. Note that in this particular case the temperature parameter of the Boltzmann distribution representing the higher rotational states is smaller than the temperature parameter of the Boltzmann distribution corresponding to the low rotational levels.

Penning ionization of many molecules is possible by helium metastables, due to the large internal energy (19.8 eV) of the $He(2^3S)$ state. Richardson and Setser [58] have reported

on the production of N_2, CO, O_2, HCl, HBr and Cl_2 ions in their excited states. The rotational populations of $N_2^+(B)$, $CO^+(B)$, $HBr^+(A)$ and $HCl^+(A)$ are found to be very similar to those of the neutral precursor molecule. At room temperature, the rotational temperature of $N_2^+(B)$ was 30 to 50 K larger than the gas temperature, in correspondence with the result from the study presented in figure 5. Interestingly, at 77 K, a non-Boltzmann distribution was found for $N_2^+(B)$. In addition, excitation from $N_2^+(X)$ to $N_2^+(B)$ by highly vibrationally excited nitrogen molecules has been suggested by Linss to produce a non-thermal rotational population distribution [59].

4.2. Production of excited states through dissociation

Dissociation of polyatomic molecules can lead to the production of electronically excited diatomic molecules, which can lead to UV and visible emission. The dissociation process can add a significant degree of complexity to the above described process of excitation and ionization. In many dissociation processes, apart from the reaction products an excess of energy is present. This excess energy can be redistributed between the different degrees of freedom of the products, i.e. translation, rotation, vibration and excitation. Dissociation often can lead to a significant ro-vibrational excitation. This is relatively easy to understand by the following simplified classical considerations. The distance between two atoms in the polyatomic parent molecule can be significantly larger in comparison with the distance in the product diatomic molecule. In this case, the Franck–Condon principle will ensure that the fragment production is favored for large vibrational excitation. One can thus state that the vibrational excitation of the dissociation product can provide information on the bond length of the molecule during the dissociation path.

In a similar classical view, one can consider that the nascent rotational distribution of the produced diatomic molecule will be strongly determined by the change in the bond angle along the dissociation path. Indeed, rotational excitation can take up the change in angular momentum. If one would consider a linear molecule which dissociates along its axis, no significant rotational excitation would be necessary to take up the change in angular momentum. In models of dissociation conditions, it is sometimes assumed, for this reason, that the dissociation occurs along a linear trajectory so that vibrational excitation without rotational excitation has to be considered (see, e.g., [60]). For more details on this topic the reader is referred to the book by Schinke [61].

4.2.1. Photo-dissociation. Photo-dissociation of polyatomic molecules producing diatomic molecules in an excited state is often studied to investigate the dissociation pathways and molecular band structures of the parent molecule. The fragmentation mechanism/pathway strongly influences and determines the rotational distribution of the product molecule. Photo-dissociation is often seen as a two-step process consisting of absorption of a photon with the production of an excited (unstable) molecular state and the dissociation of this state. The final product state distributions will depend both on the absorption and subsequently the dissociation process. Both the potential energy surfaces of the unstable excited state and the intermolecular forces acting on the product fragments during the dissociation significantly influence and determine the rotational distribution of the final molecular product. The nascent rotational distribution is in this case not related to a kinetic temperature.

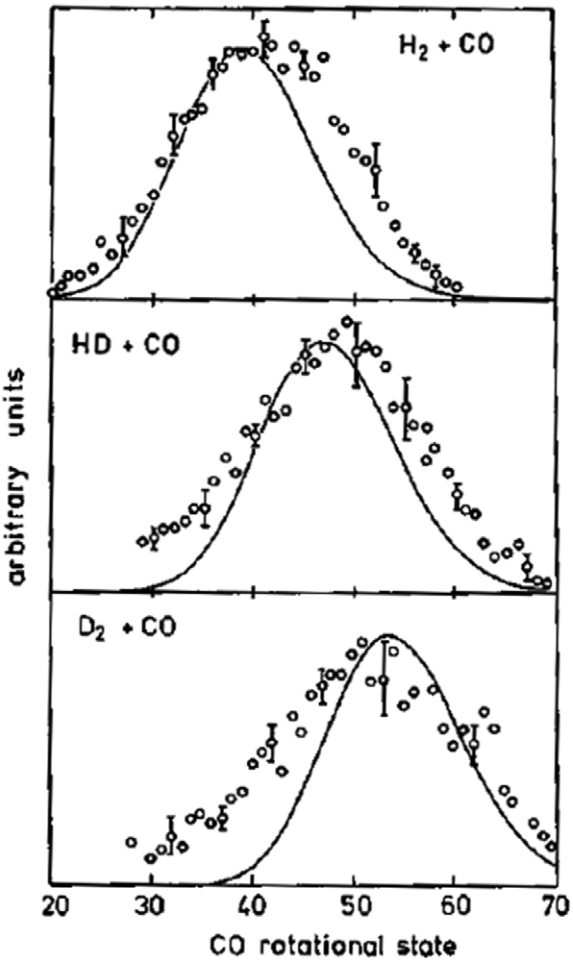

Figure 7. Nascent rotational distributions of CO following the photolysis of H_2CO, HDCO and D_2CO, respectively. Measured values are compared with theoretical predictions [62].

Examples of CO rotational distributions obtained by photo-dissociation of H_2CO, HDCO and D_2CO are shown in figure 7. This figure clearly illustrates the influence of the parent molecule and thus the different inter-atomic and molecular forces during the fragmentation process on the rotational distribution of the CO product fragment. There is an extensive literature on photodissociation and the internal rotational distributions of the products. Examples include radicals and molecules such as OH (from H_2O and H_2O_2), NO, HF, HBr, H_2 and NH [63–69].

4.2.2. Electron induced dissociation/dissociative excitation. Dissociation of polyatomic molecules can be induced by energetic electrons instead of photons. The process is very similar to the photon-induced excitation in which the formed excited state of the parent molecule subsequently dissociates.

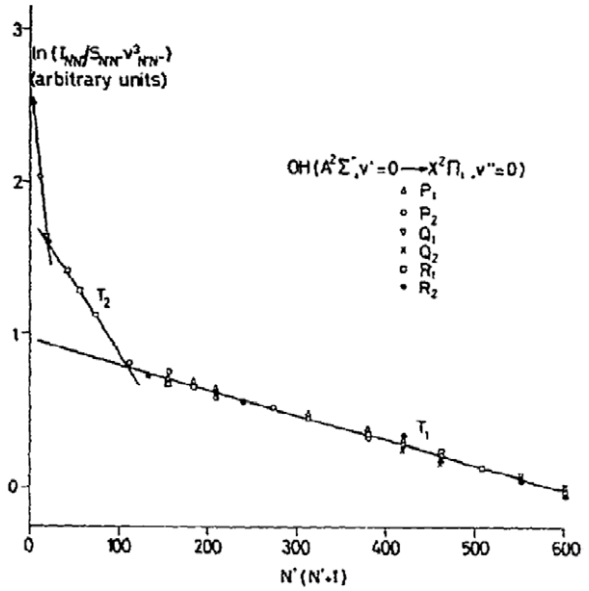

Figure 8. Nascent rotational distribution of OH(A) produced by electron-impact dissociative excitation of water vapor in an electron beam [70]. The rotational distribution can be fitted with a superposition of three Boltzmann distributions with three different temperature parameters.

As electrons in plasmas often have a broad energy distribution, several different excited states can potentially be produced of which one or more could contribute to the production of the electronically excited diatomic molecule. Each pathway can potentially produce a different rotational distribution of its product molecules.

A typical example of a commonly occurring process in plasmas is the electron dissociative excitation of H_2O to form OH(A) [70, 71]. This process has been studied with a monoenergetic electron beam. An example of the rotational distribution obtained from the emission spectra of the OH(A–X) transition is shown in figure 8. It is possible to fit the distribution by three superimposed Boltzmann distributions. Mohlmann *et al* suggested that the three rotational distributions originate from different dissociation pathways [70].

Electron-induced dissociative excitation has been investigated for many systems including CH(A) formation from acetylene, NH(A) formation from NH_3 and CO from CO_2 [72–74]; just to mention a few molecular systems which are of interest in non-equilibrium plasmas. All nascent rotational distributions show significant rotational excitation and can be fitted with a single Boltzmann distribution or the superposition of several Boltzmann distributions.

4.2.3. Dissociative recombination. As shown above, diatomic fragments produced from the dissociation of polyatomic molecules are often produced with strong ro-vibrational excitation. It is thus to be expected that dissociative recombination of polyatomic ions with an electron can also lead to ro-vibrational excitation. An example reported in [75] is the H_2O^+-electron recombination which produces OH(A) with significant ro-vibrational excitation. The low-resolution spectra obtained in [75] could be fitted assuming a Boltzmann distribution for the rotational levels with a temperature parameter of 4000 K for both $v = 0$ and 1. A nice example to illustrate that dissociative recombination can be an important production mechanism in plasmas is the dramatic enhancement of OH(A–X) emission in a recombining hydrogen plasma [76]. The production of H_2O, due to chemical etching of the glass tube surface by H atoms and subsequent ionization is proposed to be the most likely origin of H_2O^+ in the hydrogen plasma. In addition, the effective rotational temperature of OH(A) is 4200 K (very similar to the value obtained by Sonnefroh *et al* [75]) while the translational temperature measured from the hydrogen atoms (measured in the ionizing plasma) is only 2000 K.

The production of electronically excited CO from dissociative recombination of the CO_2^+ ion with an electron has also been investigated. Depending on the reported excited state, nascent rotational distributions with temperature parameters ranging from 400 to 1000 K are found under room temperature conditions. Nonetheless, the main excess energy in the dissociation reaction is stored in vibrational excitation [77, 78] and the nascent rotational distributions strongly depend on the vibrational level [78]. Anomalously large rotational excitation of CO has been found in low-pressure glow discharges and was attributed to the dissociative electron recombination of the cluster $(CO)_2^+$ ion [79]. Dissociative recombination is an important mechanism for non-equilibrium distributions, in particular for recombining plasmas with high electron densities.

4.2.4. Ion–molecule reactions. Ion–molecule reactions are of overwhelming importance in the interstellar medium and in many laboratory plasmas [80]. This is due to the absence of a repulsive barrier in most or all ion molecule reactions. In many dilute astrophysical plasmas the circumstances are different from plasma chemistry with much lower heavy particle temperature and densities. Examples are dark clouds and diffuse clouds with neutral densities in the range 10^8–$10^{10}\,m^{-3}$ and temperature as low as 10 K. The ionization degree is low and can be in the range 10^{-6}–10^{-7} [60, 81]. Time constants and length scales are thus vastly different compared with conventional laboratory plasmas. Ion–molecule and charge transfer reactions as the proton transfer and dissociative recombination are important in astrochemistry because of the low heavy particle temperatures. An important example is the H_3^+ ion which is of significant interest for astrochemistry. H_3^+ ions serve as a proton donor and facilitate the build-up of molecules from the atomic constituents of the early universe: $H_3^+ + C_2 \rightarrow C_2H^+ + H_2$ [82]. In this recombination reaction excess energy is present which can be channeled into ro-vibrational excitation [83]. In addition, ion–molecule reactions which are very important, particularly in plasmas, are the charge exchange reactions which have been addressed above.

4.2.5. Metastable induced dissociative excitation. In the case of OH(A–X) emission in water-containing Ar discharges, similar findings of rotational spectra consisting of seemingly two Boltzmann distributions are found [84]. The production of non-thermal rotational distributions in this case is also

considered to be due to the direct dissociative excitation of water by Ar metastable atoms. In crossed-beam experiments with Ar metastables and H_2O, rotational distributions in the product OH(A) radical resembling a Boltzmann distribution with an effective temperature of 4500 K are found [85]. In dissociative excitation of BrCN by argon metastable atoms, the nascent rotational distributions of CN(B) can also be described by a superposition of two Boltzmann distributions (with an overpopulation of high rotational levels) [86].

4.2.6. Dissociative charge transfer. Dissociative charge transfer can occur in the reaction of He^+ with H_2O, producing ro-vibrationally excited $OH^+(A)$ with considerable rotational excitation [87]. The OH(A–X) emission originating from the reaction of Ar^+ with H_2O and producing ArH^+ and OH(A) has also been studied [88]. To obtain a good fit of the rotational spectrum, a superposition of two Boltzmann distributions is necessary, with temperature parameters depending on the collisional energy [88].

4.3. Chemical and neutral induced dissociation reactions

Chemical reactions can also lead to the production of rotationally excited molecules. Examples of chemical production mechanisms of ground state OH(X) include $O(^1D) + H_2O \rightarrow 2OH$ and reactions of atomic oxygen with hydrocarbons. Tanaka *et al* [89] studied the water dissociation reaction by different isotopes of the $O(^1D)$ metastable oxygen atom and found that the process occurs due to H abstraction. The newly formed OH in the $v = 0$ level has a rotational temperature parameter of 6000 K while the OH remaining from the parent water molecule has a T_r of 2600 K. Both temperature parameters depend on the vibrational level. The chemical reactions which produce OH from hydrocarbons have been shown to be able to yield rotational distributions of the OH(X), which can be described by the superposition of two Boltzmann distributions [90, 91]. Similar studies have been performed for other molecules, such as NH(X) [92], HD [93] and NaH [94] which originate from dissociation reactions. The above examples are molecules/radicals produced in the ground state but they can also be produced in the excited state. An example is the CH(A–X) emission in the chemical reaction of C_2H and $O(^3P)$ [95].

4.4. Surface reactions

Surface association reactions of atoms can also lead to ro-vibrationally excited molecules. It is found by Creighan *et al* [96] that both H_2 and HD can be produced with rotational distributions which significantly exceed the temperature of the graphite surface at 15–50 K. These processes are of importance for astrochemistry and therefore a significant amount of information is available at these low temperatures. It must be stated that the opposite (reduction in rotational excitation or rotational cooling) has also been observed on a Pd surface [97]. For surface reactions, there exists a model of so-called hindered rotational states for molecules adsorbed on surfaces. Basically, one of the atoms is fixed to a surface and the solid angle in which the molecule can freely rotate is restricted. From this model, the obtained rotational population distribution is very similar to the typical rotational distributions with an overpopulation of high rotational levels as observed in dissociative processes occurring in plasmas [98]. The very detailed H_2, D_2 and HD ro-vibrational distributions measured by Gabriel *et al* [229] are an example of the possible influence of surface reactions in recombining plasmas.

4.5. Important remark on nascent distributions

An important observation is that in many cases, the nascent rotational population distributions can be fitted with a Boltzmann distribution or with the superposition of several Boltzmann distributions, in spite of the fact that this is not *a priori* to be expected. The temperature parameters of the nascent distributions do not have any meaning as a kinetic temperature. As a consequence, observing a rotational Boltzmann distribution is a necessary but not sufficient condition for assuming that the rotational distributions are in equilibrium with the gas kinetic temperature. This representation of the rotational level densities by the well-known Boltzmann distribution is useful but can be a source of error when it is automatically interpreted as a rotation–translation equilibrium in non-equilibrium plasmas. Note that in the majority of cases shown, an overpopulation of high rotational states occurs, which in the absence of thermalization of the rotational states would typically lead to a larger rotational temperature parameter in comparison with the gas temperature. Nonetheless, there are a few exceptions, as in the case of the CO(X; $v = 1$) shown in figure 6 and with excitation transfer from metastable atoms with energy constraints as described above.

5. Additional effects influencing rotational population distributions

When one is observing the emission from an excited state produced by a reaction which is known to populate rotational levels with a specific rotational distribution, the RET is of course of key importance in the interpretation of the observed rotational distribution. The rotational distribution can represent an imprint of the formation process, a representation of the kinetic temperature or a combination of both. In addition, all level-specific parameters which can depend on the rotational quantum number, such as the effective lifetime or the collisional transfer properties, can influence the rotational population distribution. In this section, a small comment is also made on the transition probability dependence of the rotational states.

5.1. Level-dependent cross-sections for RET

RET can depend on the rotational number and may strongly influence the thermalization time of the rotational states. It is important to note that the thermalization time is also determined by the nascent rotational population distribution (at least the amount of its deviation from equilibrium). If the nascent rotational population distribution is far from the thermalized Boltzmann distribution, thermalization by

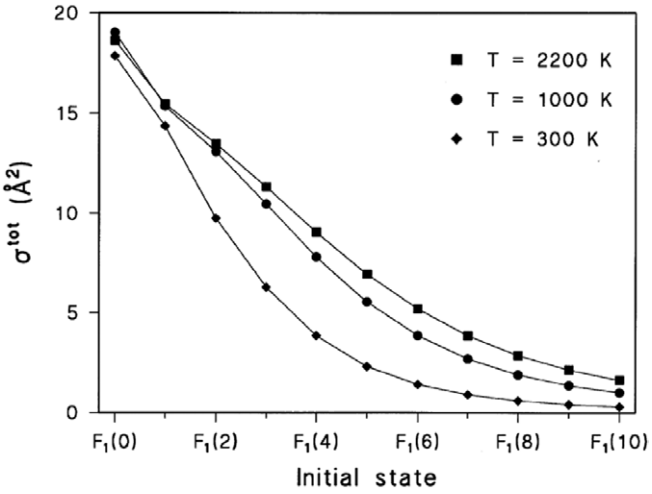

Figure 9. Calculated total RET cross-section for OH(A) in collisions with He as a function of the initial level and the gas temperature [99].

collisional transfers between rotational levels needs to occur in order to measure the gas temperature. An example of the dependence of the total RET cross-section on the rotational number for OH(A) is shown in figure 9. From this figure it is clear that the RET cross-section changes by almost a factor of 60 between $N = 1$ to $N = 10$. Given such a strong dependence on the rotational quantum number of the rotational transfer rate, it is logical to consider different time scales for the thermalization of different parts of the rotational population distribution. As a general rule, RET rate coefficients tend to zero when with increasing rotational number J, the energy gap between the rotational levels becomes comparable or larger than kT_g, the kinetic energy.

The above effect can be easily understood by the following simplified treatment taken from [100]. State-to-state RET coefficients (k_{if} ($J_i \rightarrow J_f$)) have been extensively measured for different diatomic molecules. Several scaling laws (see, for example, [99]) have been proposed including a power scaling law $k_{if} \propto \Delta E_{if}^{-\gamma}$ with γ a positive constant. Assuming $\gamma \approx 1$ and considering that $\Delta E_{if} \approx 2BJ_i\Delta J$ one reaches the conclusion that the state-to-state RET rate scales with $1/(J_i\Delta J)$. The most important collisional transfers end in the neighboring rotational levels, with small ΔJ values. This also clearly illustrates the observed faster-reached population equilibrium for small J_i levels in comparison with large ones. This effect will be further increased (as is illustrated in figure 9) by the fact that the total RET rate (summed RET rate out of a single level) will be larger at small J_i because there is a larger availability of J_f levels due to the small energy gap between the levels.

The rotational level-dependent RET has also been measured for e.g. CH(A) [101], CN(X) [102] and NO(A) [103]. Note that the dependence on rotational level is typically more pronounced for the molecules with a low reduced mass, i.e. containing a H, like CH and OH, compared with molecules with a large reduced mass like NO. This is mainly due to the larger rotational constant B in the former molecules which results in much faster enhancement with J_i of the energy

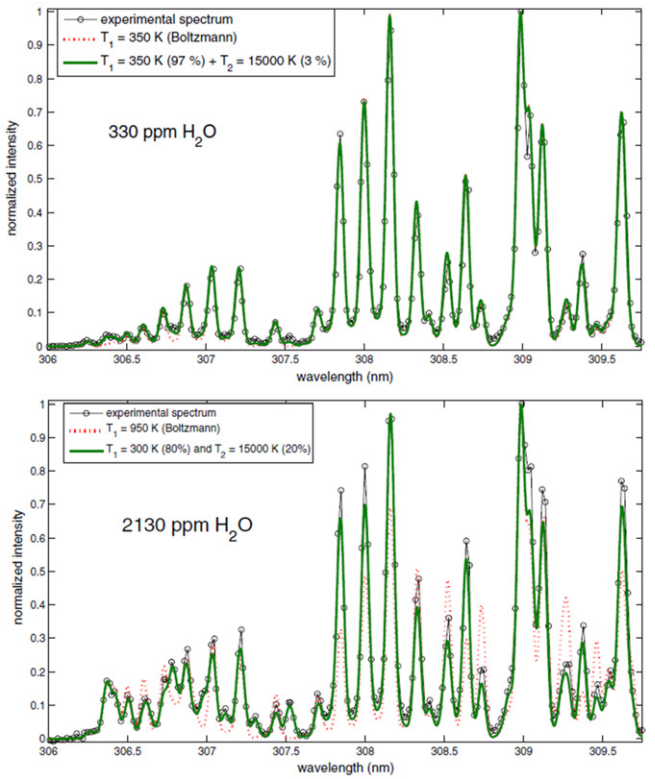

Figure 10. Emission spectrum of OH(A–X) and corresponding fits obtained in an atmospheric pressure glow discharge with two different water concentrations. The remnants of the nascent non-Boltzmann distribution is in this case even observed at atmospheric pressure due to the significant collisional quenching and the consequent reduction of the effective lifetime of the OH(A) state. The gas temperature remains constant within 350 ± 50 K [105].

gap between levels. Note that the gas temperature can have a significant effect on the RET rates and thermalization as recently shown for NO(A) [104].

In the rest of this section, two examples for which RET is an important factor in the experimentally observed rotational population distribution are presented. An enhancement of the overpopulation of high rotational levels of the excited electronic state OH(A) has been observed in a diffuse atmospheric pressure RF glow discharge operating in He–H_2O mixtures when the water vapor pressure was increased [105]. Note that due to the large collisional quenching rate of OH(A) by H_2O, an increase in the H_2O concentration leads to a reduced effective lifetime of the OH(A) state. When the spectrum is fitted with the superposition of two Boltzmann distributions, the temperature parameter corresponding with the lower rotational levels is found to be close to the gas temperature (see figure 10). Indeed, the low rotational levels have faster RET rates compared with the higher rotational states, in spite of the reduced effective lifetime; the He–OH(A) collision frequency in low rotational levels is high enough to lead to a Boltzmann equilibrium at the He gas temperature while this is not the case for the high rotational levels. The levels with large rotational numbers still reflect, to a large extent, the nascent rotational distribution of their production mechanism. In this particular case, with an electron density of the order of 10^{17} m^{-3} and water present as an impurity,

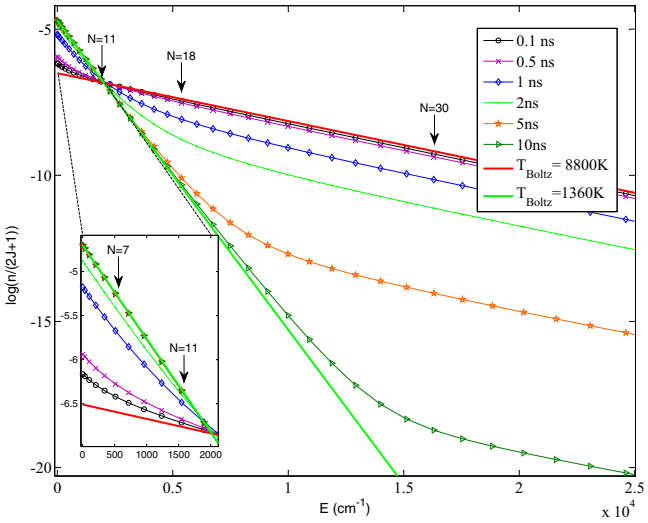

Figure 11. Rotational population distribution of OH(A) at different times after their production in pure water vapor at 1360 K. It is assumed that the nascent OH(A) rotational populations is a Boltzmann distribution with a temperature parameter of 8800 K. The equilibrium Boltzmann distribution at a gas temperature of 1360 K is also included in the figure (solid green line) as a reference.

OH(A) is mainly produced by the dissociative recombination of electrons with water ions or by Penning ionization of trace water molecules by He_m (see also [106]). On the other hand, if water is present at larger amounts, the electron-impact dissociative excitation of water dominates the OH(A) production. Note that both dissociative e–ion recombination of the water ion and the electron dissociative excitation of water are processes which produce nascent rotational population distributions with high rotational excitation (see above).

A second example is presented to illustrate that RET can also cause a two-temperature distribution even if the nascent rotational distribution can be fitted with a single Boltzmann distribution. As an illustrative example we approach the experimental conditions of the result presented in figure 1. Kienle *et al* [99] have published an RET fitting model which is validated by RET rate measurements of OH(A) by water at 1360 K. The fitting model, which is a so-called ECS-P model (energy corrected sudden power law model, which describes the correlations used to obtain the RET rates for different rotational levels, see [99] for details), allows one to obtain RET rates for all rotational levels of the OH(A) $v = 0$ rotational manifold. Note that 1360 K is close to the estimated gas temperature of 1550 K in figure 1. At least, qualitative information on the experimental conditions of figure 1 can be obtained with this approach.

The different OH(A) rotational population distributions as a function of time after their production are calculated starting from a nascent OH(A) Boltzmann distribution with a temperature parameter of 8800 K. The used RET rates are obtained as described above. As mentioned above, the RET rate decreases with increasing rotational number. This means that the lower rotational levels reach equilibrium with the gas temperature much faster than the high rotational levels. As can be seen in figure 11, this effect leads to the formation of a hockey-stick shaped distribution which, in some cases, can be approximated by the superposition of two Boltzmann distributions. This result shows that in strongly collisional high-pressure plasmas, when RET is fast, the shape of the rotational distribution in the excited states of molecules is significantly, if not strongly, influenced by the RET. Note that in this specific case, it takes approximately 1 ns for the rotational levels up to $N = 7$ to thermalize, while 10 ns is necessary for rotational levels around $N = 20$. When the strongly collisional quenching reduces the effective lifetime of the excited state to about 1 ns, as in the case of the atmospheric pressure plasma of figure 1, population of the high rotational levels still exhibit remnants of the nascent distribution and provide an image of the formation process.

Similar findings of partly thermalized rotational distributions at atmospheric pressure have been published for CH(A–X) emission by Luque *et al* [107] and for $N_2(C)$ by Wang *et al* [100]. It must be emphasized that effects on the rotational distribution function by level-dependent cross-sections of RET can be very important in atmospheric pressure plasmas and in several cases, the lower rotational levels allow estimation of the gas temperature [100]. In this case, it is possible to accurately fit a multiple Boltzmann distribution or make Boltzmann plots which allow an accurate temperature measurement when a sufficiently high-resolution rotational spectrum is available (see also below).

5.2. Effective lifetime dependence on rotational states

The emission intensity from a rotational level is proportional to the product of the density in this level by the Einstein A coefficient of the observed line:

$$I_{J'J''} \propto n_{J'} A_{J'J''} \nu_{J''J'}. \tag{8}$$

Under steady-state conditions, the density $n_{J'}$ is related to the population term of the level, $S_{J'}$, the line strength, and its effective lifetime, $\tau_{J'}$, and the above equation can be rewritten as

$$I_{J'J''} \propto n_{J'} \nu_{J'J''} A_{J'J''} = S_{J'} \nu_{J''J'} A_{J'J''} \tau \tag{9}$$

$$= S_{J'} \nu_{J''J'} \frac{A_{J'J''}}{\Sigma_{v''J''} A_{J''J'} + \Sigma_i k_{q,i,v'J'} n_i + A_{pd}}. \tag{10}$$

The effective lifetime $\tau_{J'}$ is determined by the Einstein A coefficient ($A_{J'J''}$), the collisional quenching ($k_{q,i}$) and the pre-dissociation rates (A_{pd}). Collisional quenching is important for high density and high-pressure plasmas and the quenching rate can depend on the rotational level (see, for example, the case of OH(A) [108]). Pre-dissociation can be important, for example, for OH(A) or NH(A and c) [109]. It usually becomes more important for increasing vibrational number as the energy gap between the dissociation limit and the energy of the level reduces with increasing vibration number. Reported values indicate that in the OH(A) $v' = 0$ state, for $N > 20$, the pre-dissociation rate equals the fluorescence rate [110].

For several molecules, the lifetime dependence of rotational states can be safely ignored. For example in the case of $N_2^+(B)$, the radiative lifetime of the rotational levels between $N' = 0$ to 50 varies only by 5% [111].

The effect of the lifetime is often neglected in the literature. This is often a good approximation when only a limited number of rotational lines, far from the pre-dissociation limit, is considered, and if the dependence on collisional quenching of the rotational level is not important.

5.3. Transition probability dependence of rotational levels

The intensity of emission from a given rotational level J' is defined as $I_{J'J''} \propto n_{J'} A_{J'J''} \nu_{J''J'}$ with

$$A_{J'J''} = \frac{g'_e}{g''_e} \frac{64\pi^4}{3h} \frac{S^{J'}_{J''}}{2J'+1} p^{\nu'J'}_{\nu''J''} (\nu^{\nu'J'}_{\nu''J''})^3. \quad (11)$$

In this formula $p^{\nu'J'}_{\nu''J''}$ is the ro-vibrational transition probability, $S^{J'}_{J''}$ is the Hönl–London factor or line strength, $g_e = (2 - \delta_{0,\Lambda})(2S + 1)$ with S being the state spin multiplicity and $\delta_{0,\Lambda} = 1$ for Σ states while 0 for all others. When dealing with only the relative intensities of rotational lines belonging to the same vibrational band, one can often find in the literature the following relation for the relative intensities:

$$I_{J'J''} \propto n_{J'} \frac{S^{J'}_{J''}}{2J'+1} (\nu^{\nu'J'}_{\nu''J''})^4, \quad (12)$$

which uses the line strength $S^{J'}_{J''}$ rather than the Einstein A coefficient ($A_{J''J'}$). This, however, assumes that the ro-vibrational transition probability ($p^{\nu'J'}_{\nu''J''}$) does not depend on the rotational level. This assumption, for example, is correct for the $N_2^+(B)$ state (for which an example using $S^{J'}_{J''}$ factors is shown in figure 5) but not for the OH(A) state [111]. It is thus better, when available, to use the Einstein A coefficients.

For the NH(A; $\nu = 0$) radical, Smith *et al* have observed an enhancement by about 15% of the lifetime between rotational levels $N = 4$ and $N = 25$ of $\nu = 0$ vibrational level. They have attributed this variation to the decrease in the transition moment with increasing centrifugal distortion of the molecule [109]. The very sharp decay of the lifetime for rotational levels above $N = 25$ (τ divided by 5 for $N = 31$) was attributed to the pre-dissociation via interaction with $A\,^3\Pi$ and $^5\Sigma^-$ states. The same trend was also observed in NH(A; $\nu = 1$), with τ reaching 10% of its low rotational value at $N = 24$. These authors have also measured the lifetime of the NH($c^1\Pi$; $\nu = 0, 1$) state, which for $\nu' = 0$ changes significantly up to $N = 8$ and hence slowly decreases up to $N = 16$, but a sharp lowering of the τ was observed for $\nu' = 1$ level [109]. The conclusion of these authors was that the $^5\Sigma^-$ state, resulting from the ground state asymptote, should be responsible for the observed pre-dissociation in the $c^1\Pi$ state, via spin–orbit or spin–spin coupling [109].

6. Commonly used excited states for the determination of the gas temperature by OES

The detailed analysis of excited states commonly used to determine the gas temperature by OES will be restricted to the following transitions: $N_2(C–B)$, OH($A–X$) and $N_2^+(B–X)$. These transitions nicely cover three different cases: a molecule which is part of the feed gas, a molecule which, in most cases, is formed by a dissociation process in the plasma and an ionic transition.

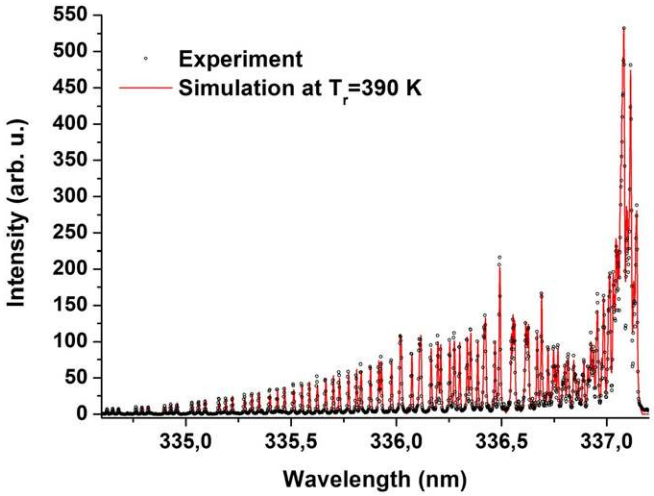

Figure 12. High-resolution (4 pm, FWHM) rotational spectrum of the $N_2(C–B;0–0)$ vibrational band recorded in a RF He–H_2O diffuse glow discharge at atmospheric pressure containing air impurities [9].

6.1. $N_2(C)$

The $N_2(C\,^3\Pi_u–B\,^3\Pi_g)$ system, which is also called the second positive system of nitrogen, is often responsible for the dominant emission in air or N_2-containing plasmas. Its different vibrational branches range between 280 and 500 nm with the head of the (0,0) vibrational transition at 337 nm [117]. Most often, the (0,0) transition or the (0,2) transition at 380 nm is used to obtain the rotational temperature. Both upper and lower electronic states are $^3\Pi$, thus having three sub-states each and with increasing J number evolve from case a to case b of Hund [18], with Λ-doubling of rotational levels. The transition contains 27 branches, 9 of them being the principal ones and sharing the essential intensity of high N' levels. Hönl–London coefficients for all 27 branches are given in [16]. The spectroscopic constants of the transition can be found in [19, 20, 118]. For very high-resolution spectroscopic studies, one should use spectroscopic constants deduced by Roux *et al* [119]. An example of a high-resolution rotational spectrum of the $N_2(C–B;\ 0–0)$ vibrational band is shown in figure 12.

Observing the $N_2(C–B)$ emission from a plasma is an indication that N_2 is present in the plasma reactor because the excitation is usually not induced by a dissociation process. Moreover, beside the direct electron-impact excitation from the ground state, several other production mechanisms can be responsible for the population of the $N_2(C)$ state. An overview of the production mechanisms of $N_2(C)$ is given in table 1. In the case of electron excitation, one should compare the rotational constants of the parent and product state. The rotational constants of the X, A and C states are 1.998, 1.455 and 1.825, respectively [118]. In particular, in the case of excitation from the metastable $N_2(A)$ state, the temperature deduced from rotational lines of the $N_2(C)$ state using the rotational constants of the $N_2(C)$ state could be underestimated if no RET occurs in this state.

The production mechanisms of $N_2(C)$ have been studied in a pulsed RF discharge in the range of 0.1–3 Torr by De

Table 1. Production reactions for $N_2(C)$ and the corresponding rate coefficients. Electron excitation reactions are calculated from the cross sections in the given references assuming a Boltzmann EEDF.

Reaction	Typical rate k ($m^3\ s^{-1}$)	Remark	Ref.
Electron excitation			
$e^- + N_2(X) \rightarrow e^- + N_2(C)$	1.3×10^{-19}–2.7×10^{-16}	$T_e = 1$–3 eV	[112]
		$E_{ex} = 11.0$ eV	[113]
$e^- + N_2(A) \rightarrow e^- + N_2(C)$	5.6×10^{-16}–2.7×10^{-14}	$T_e = 1$–3 eV	[112]
		$E_{ex} = 4.9$ eV	[113]
Metastable excitation			
$N_2(A) + N_2(A) \rightarrow N_2(C) + N_2(X)$	1.5×10^{-16}	—	[114]
$Ar(^3P_2) + N_2(X) \rightarrow N_2(C) + Ar$	3.6×10^{-17}		[115]
Dissociative recombination			
$N_4^+ + e^- \rightarrow N_2(C) + N_2(X)$	2.6×10^{-12}	—	[116]

Benedictis and Dilecce [120]. It is found that in the discharge, the $N_2(C)$ is predominantly produced by $N_2(X)$ excitation. In the late afterglow, when the electron temperature dropped down to the gas temperature, the pooling reaction of $N_2(A)$ becomes the most important. However, in the early afterglow there can still be a contribution from the electron excitation of the $N_2(A)$ metastable state. Note that the rate coefficient for the electron excitation from $N_2(A)$ is only about two orders of magnitude higher than the direct excitation from the ground state. As a consequence, in most ionizing plasmas, it will not be a dominant process. A similar study for a corona discharge at atmospheric pressure is performed by Simek *et al* [121]. The main difference is that in this case, due to the faster drop in T_e at higher pressures, which quickly reduces the rate of electron excitation, the afterglow production of $N_2(C)$ is dominated by the pooling reaction.

Note that the rate for $N_2(X)$ excitation by $Ar(^3P_2)$ is about five times smaller than the $N_2(A)$ pooling reaction. As in many cases the $N_2(A)$ density is much smaller than the ground state $N_2(X)$ density, excitation transfer from Ar metastables is often a very important production mechanism of $N_2(C)$. Isola *et al* [122] found a significant contribution of Ar metastable excitation at low pressures when more than 50% N_2 was present in the reactor. If instead of pure nitrogen air is considered to be the impurity present in argon, at 25% of its amount the excitation rates of $N_2(C)$ by direct electron impact and by energy transfer from Ar metastables become almost equivalent. The difference is due to the about six times larger quenching rate of $Ar(^3P_2)$ by O_2 than by N_2 [123]. As shown above, the Ar metastable excitation leads to a nascent rotational distribution with large rotational excitation. It is suggested, based on indirect information, that the production of $N_2(C)$ by pooling could potentially also produce high rotational excitation [124, 125].

The dissociative recombination reaction of N_4^+-producing $N_2(C)$ is also reported [116]. However, as is shown, e.g., in a glow discharge at atmospheric pressure, N_3^+ and N^+ are dominant ions. In this particular case, while associative ionization reactions producing N_4^+ are the dominant ionization processes in the discharge, the dominant ionic recombination losses are due to the dissociative electron recombination of N_3^+ [126]. In low-pressure glow discharges, it is also found that N_4^+ is not the dominant ion [127]. At low pressures, the electron temperature is large, causing important electron excitation of $N_2(A)$ during the plasma on phase. The metastable molecules can be very important in the afterglow. In most cases the production of $N_2(C)$ by dissociative recombination will thus not be important.

In a low-pressure CCl_4 discharge, a comparative study has been made between the rotational temperature (obtained from LIF) of the ground state CCl molecule in equilibrium with the gas temperature and T_r of $N_2(C)$ when N_2 was added as an actinometer gas [128]. The conclusion was that the $N_2(C–B)$ emission can be used to measure the gas temperature, provided such measurements are performed in the bulk of the plasma and not in close proximity to surfaces. Examples of such measurements can be found, e.g., in [129]. This example illustrates the reliability of the $N_2(C–B)$ emission for the gas temperature measurements even in plasmas with complex gas mixtures and chemistry.

With exclusion of Ar-containing plasma and the above-mentioned production of $N_2(C)$ by the pooling reaction of $N_2(A)$, only few results can be found in the literature for which the $N_2(C)$ system seems to have a rotational population distribution that is not in equilibrium with the gas temperature. Based on indirect evidence, it is suggested in [130] that $N_2(C–B)$ emission in N_2O plasmas (even at atmospheric pressure) can also suffer from high rotational excitation. In this case N_2 is produced in dissociation processes which indeed could lead to a high ro-vibrational excitation. In [131], the rotational temperature of N_2 is reported to significantly exceed the gas temperature, although the presented spectrum seems to have a contribution from the $NH(A–X)$ system, which could also cause the excessive estimated rotational temperature. In fact, the presence of this $NH(A–X)$ band was not taken into account in the analysis.

In the case that a non-thermal nascent rotational population distribution is expected, e.g. when Ar_m excitation is the dominant production mechanism of $N_2(C)$, it is necessary to estimate the rotational thermalization time and the effective lifetime of the $N_2(C)$ state. The collisional quenching rates with various colliding partners are summarized in table 2, which allow calculation of the effective lifetime of $N_2(C)$ for most plasma conditions. Note that the radiative lifetime of the $N_2(C)$ state is 36 ns. Actually, in a nitrogen environment at 300 K and 1 bar, the lifetime reduces to 3.3 ns while in air under the same conditions the effective lifetime is only 0.6 ns.

Table 2. Quenching rates for $N_2(C;\, v = 0)$ by different species.

Reaction	k ($m^3\ s^{-1}$)	Ref.
$N_2(C) \rightarrow N_2(B) + h\nu$	$2.74 \times 10^7\ s^{-1}$	[132]
N_2	1.1×10^{-17}	[133]
O_2	3.0×10^{-16}	[134]
H_2O	3.9×10^{-16}	[134]
H_2	3.3×10^{-16}	[134]
CO	2.4×10^{-16}	[135]
Ar	3×10^{-19}	[136]

Table 3. Rotational–translational relaxation times and Z_r values for $N_2(X)$. The values are given for 300 K and atmospheric pressure if not stated otherwise.

Collision partner	τ 10^{-10} s	Z_r	Remarks	Ref.
N_2	5.8	4		[138]
	7.4–12	5–9		[139]
	5.9	4		[140]
	5.9–21	4–15	300–1300 K	[141]
	5.2–10.9	4–8	200–2000 K	[142]
He	4.5–10.3	4–9		[138]
Ar	4.1–5.8	3–4		[138]
	32	20		[137]

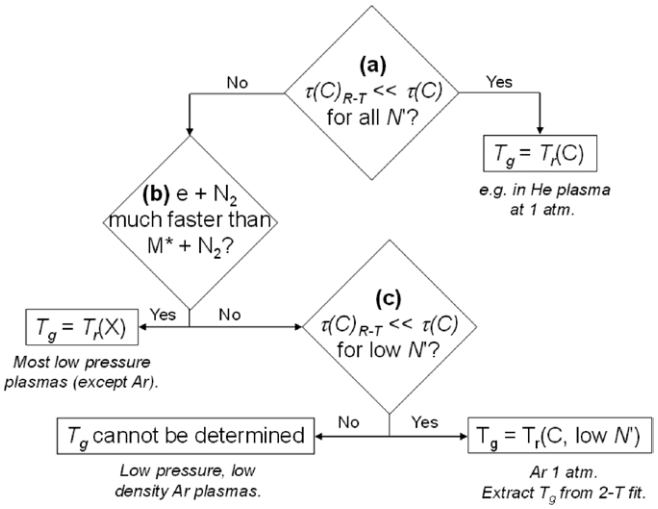

Figure 13. Flow chart indicating which conditions apply in the determination of the gas temperature, T_g, from the $N_2(C–B)$ emission bands. $\tau(C)$ is the lifetime of the $N_2(C)$ state, including quenching, $\tau(C)_{R-T}$ is the time for C-state rotation to gas translation thermalization, $T_r(C)$ and $T_r(X)$ are the C-state and ground state rotational temperatures, respectively, and N' is the rotational quantum number for the C state. Adapted from [100].

A large amount of data does not exist on RET measurements in the $N_2(C)$ state. Setser *et al* [41] estimated a RET rate by collisions with argon (for $\Delta N = 1$ collisions) of $1.7 \times 10^{-16}\ m^3\ s^{-1}$ for high rotational states ($N' = 40$) in an Ar/N_2 mixture ratio of 17. This rate can be compared with the state-to-state RET rates by argon of the ground state of N_2, measured by Belikov *et al* [137] yielding values for $\Delta N = 2$ collisions between 0.24 and $1.15 \times 10^{-16}\ m^3\ s^{-1}$ at 300 K for rotational levels below $N = 12$.

For $N_2(X)$ there exist a lot of data obtained from molecular beam experiments, Raman scattering and thermal-acoustical measurements which estimate the rotation–translation energy transfer time or the total number of necessary collisions to obtain equilibrium between rotational and translational temperatures (Z_r). An overview of the rotational–translational relaxation times and/or number of collisions for equilibration is given in table 3. The large scattering in the data is immediately clear. This could be (partly) due to the different measurement conditions, which can induce large or small deviations in the rotational distribution in comparison with the translational temperature. This will of course also influence the thermalization time [137]. The main conclusion from table 3 is that thermalization typically occurs within less than 10 collisions, which corresponds to a time scale of about 1 ns at atmospheric pressure. However, experimental results such as obtained by Wang *et al* [100] illustrate that the thermalization time in the lower rotational levels of the $N_2(C)$ is significantly higher than 1 ns at atmospheric pressure. The comparable rates obtained in $N_2(C)$ by Setser ($\Delta N = 1$) for argon at $N' = 40$ and the highest rate reported for the ground state RET ($\Delta N = 2$) is in agreement with this result. In addition, using the scaling law $K_{if} \propto B^{-1}$, comparing with the thermalization time of the lower levels of $OH(A)$ in figure 11 (about 1 ns) and considering the ratio of the rotational constants of $OH(A)$ and $N_2(C)$, which is about 10, would lead to a typical thermalization time of 100 ps for the lower rotational states of $N_2(C)$. This would indeed render the thermalization of the lower rotational levels of $N_2(C)$ in air and in N_2 at atmospheric pressure possible. This result justifies the widespread use of the $N_2(C–B)$ emission to obtain the gas temperatures in atmospheric pressure plasmas.

The flow chart given by Wang *et al* [100] as included in figure 13 can be used to estimate the approach for obtaining the gas temperature from $N_2(C–B)$. Basically, at atmospheric pressure if argon is not the background gas and when the lifetime of the $N_2(C)$ state is not significantly reduced by quenching, e.g. in helium, $N_2(C–B)$ emission yields a good measurement of the gas temperature. This is also the case in low-pressure plasmas in which a maximum error of 9% can be introduced if the rotational constant of the ground state is not taken into account to deduce the gas temperature.

In conclusion, the $N_2(C–B)$ emission yields in many cases the gas temperature with the main exception being when it is observed in Ar plasmas (with a considerable metastable density such that electron excitation of $N_2(C)$ from $N_2(X)$ is no longer dominant). In argon plasmas, at low pressures no translation temperature can be obtained. At high pressures, a partial thermalization of the low rotational levels can occur and a fit using a superposition of two Boltzmann distributions can be used of which the distribution of the low rotational levels yields a good estimate of the gas temperature [43]. It should be noted that in Ar/N_2 plasmas, the $v' = 3$ and the $v' = 4$ levels of the $N_2(C)$ state are populated predominantly by electron-impact excitation, since energy transfer from the most populated $Ar(^3P_2)$ metastable state is not effective for these levels. These levels can also be chosen for the gas temperature determination if the intensity of their emission is strong enough for recording a good quality rotational spectrum [100].

Table 4. Production reactions for OH(A) and the corresponding rate coefficients. The electron-induced dissociation and attachment processes are calculated from cross-sections reported in [146], assuming that the electron distribution is Maxwellian. It is assumed that the gas temperature has a small effect on the calculation of the direct excitation reaction from the thermal rates published in [145].

Reaction	Typical rate k ($m^3\ s^{-1}$)	Remark	Ref.
Electron excitation			
$OH(X) + e \rightarrow OH(A) + e$	3.2×10^{-14}–7.5×10^{-13}	$T_e = 1$–3 eV	[145]
Electron dissociation			
$e^- + H_2O \rightarrow OH(X) + H + e^-$	2.3×10^{-18}–8.6×10^{-16}	$T_e = 1$–3 eV	[146]
$e^- + H_2O \rightarrow OH(A) + H + e^-$	1.6×10^{-19}–1.2×10^{-16}	$T_e = 1$–3 eV	[146]
Dissociative attachment			
$e^- + H_2O \rightarrow OH(A/X) + H^-$	4.8×10^{-18}–7.8×10^{-17}	$T_e = 1$–3 eV	[146]
Electron–ion dissociative recombination			
$e^- + H_2O^+ \rightarrow OH(A/X) + H$	$5.1 \times 10^{-14} T_e^{-1/2}$		[147]
$e^- + H_3O^+ \rightarrow OH(A/X) + H_2$(or 2H)	$1.05 \times 10^{-13} T_e^{-1/2}$		[148]
Positive–negative ion recombination			
$H^- + H_3O^+ \rightarrow OH(A/X) + H_2 + H$	2.3×10^{-13}	$T_g \approx 300$ K	[148]
Metastables			
$N_2(A) + OH(X) \rightarrow OH(A) + N_2(X)$	$\times 10^{-17}$		[149]
$Ar_m + H_2O \rightarrow OH + H + Ar$	4.5×10^{-16}	$T_g \approx 300$ K	[150]
Charge exchange			
$Ar^+ + H_2O \rightarrow OH(A/X) + ArH^+$	0.5×10^{-15}		[151]
$He_2^+ + H_2O \rightarrow OH(A) + HeH^+ + He$	1.3×10^{-16}		[152]

6.2. OH(A)

The OH($A\,^2\Sigma^+$–$X\,^2\Pi_i$) emission around 309 nm is ubiquitous in non-equilibrium plasmas because it is a strong transition and the presence of trace amounts of water vapor in plasma reactors is often difficult to prevent. The properties of the OH(A–X) transition and the characteristic properties of the OH(A) state have been extensively studied for years and OH(A) is probably one of the most investigated electronically excited states. The rotational lines and constants have been reported by Dieke and Crosswhite [143]. More recently, calculated rotational transition probabilities have been reported by Chidsey and Crosley [144]. The transition has 12 branches. All necessary constants of the OH(A–X) transition are included in the Lifbase database [111]. As the reduced mass involved in the rotational constant of OH is significantly small in comparison with, e.g., N_2, even with a moderately wavelength resolving spectrometer it is possible to obtain partly rotationally resolved spectra and clearly discern the band heads.

As in many cases the OH(A) is not directly produced from OH(X) by electron impact and often dissociative excitation of heavier polyatomic molecules is involved in this production; the nascent rotational distribution of OH(A) is likely to be non-thermal, often with a large rotational excitation. It is thus critical for the adoption of the OH(A) rotational temperature as the gas temperature to have detailed information on its production mechanisms. This will yield a first assessment on the expected amount of rotational excitation (and thus a measure of the deviation from equilibrium) due to the production process. In addition, together with the RET time constants and the effective lifetime of OH(A), it is necessary to determine how fast the rotational population distribution will be thermalized.

The striking resemblance of the rotational population distribution of OH(A–X) at atmospheric pressure in figure 1, with the OH(A–X) emission from the nascent population distribution produced by an electron beam excitation of water as shown in figure 8, illustrates the importance of the knowledge of the production mechanisms, effective lifetime and RET rates. In view of the many new application areas for cold atmospheric pressure plasmas in complex molecular mixtures, and even in liquid water, the above consideration becomes of increasing importance.

Several important production reactions of OH(A) encountered in non-equilibrium plasmas are summarized in table 4. Electron induced excitation from the ground state OH(X) has a significantly larger rate coefficient compared with the dissociative excitation of water, because of the threshold energy difference of 5.1 eV, which corresponds to the dissociation energy of water (excitation energy of OH(A) is about 4 eV) [153]. Comparing the rates, one can conclude that for a water dissociation degree larger than 0.1%, the direct excitation of OH(X) to OH(A) can be dominant. Similar rates for OH(A) production in the dissociative attachment reaction are expected.

When electron excitation from OH(X) is dominant, a close to thermal distribution is expected (the rotational constant of the X and A states are, respectively, 18.90 and 17.39 which will cause at maximum a 10% error if the rotational constant of the upper A state is used). Dissociative excitation of water will lead to a significant rotational excitation, as shown in figure 8.

Electron–ion recombination reactions have a rate which is typically 3 to 6 orders of magnitude higher than the rate of dissociative electron excitation of H_2O (with T_e in the range 1–3 eV). However, the branching ratios for OH and the ratio of the produced OH(X) and OH(A) depend highly on the experimental conditions. Sonnenfroh *et al* [75] showed that for a T_e of approximately 0.1 eV up to 15.6% of the electron–H_2O^+ dissociative recombination reactions lead to OH(A). The threshold branching ratios for OH(X and A) in beam experiments is 0.22. However, in an

Table 5. Quenching rates for OH(A; $v = 0$) by different species and the thermalization time constants for OH(X) rotational distribution as produced by H_2O_2 photolysis rescaled to units atm. ns.

Reaction	k ($m^3\ s^{-1}$)	Therm. time (atm ns) ($N \leqslant 13$)	Ref.
OH(A) $\rightarrow$ OH(X) + $h\nu$	$1.45 \times 10^6\ s^{-1}$	—	[157]
N_2	2.8×10^{-17}	18	[158]/ [159]
O_2	1.4×10^{-16}	19	[160]/ [159]
H_2O	7.2×10^{-16}	4	[160]/ [159]
H_2	1.8×10^{-16}		[160]
CO_2	4.0×10^{-16}		[160]
CH_4	2.8×10^{-16}		[160]
OH	6.2×10^{-16}		[160]
Ar	$\leqslant 0.03 \times 10^{-17}$	21	[161]/ [159]
He	$\leqslant 1.5 \times 10^{-20}$		[152]

afterglow, branching ratios for OH of 0.55 are found [147, 154]. Similarly, the dissociative electron–H_3O^+ recombination produces predominantly OH(X and A). A branching ratio of 0.77 was found in a storage ring [155]. Electron–cluster ion recombination can also produce OH radicals but to our knowledge no information on branching ratios for OH(A) production is published [156]. It is emphasized that electron–ion recombination reactions are important only in high (electron) density plasmas. Similar arguments are valid for the ion–ion recombination.

Note that in table 4, for the metastable reactions with H_2O, He_m is not included as it will normally lead to the ionization rather than to the production of OH(A). This is due to the large excess in energy of the most populated He($^3S_1$) metastable state (19.8 eV) in comparison with the ionization energy of water (12.6 eV) (see also [106]). Metastable-induced (dissociative) excitations are generally important when water is present as a trace compound, especially in the afterglow of pulsed discharges.

The dissociative charge transfer reaction with Ar^+ has an excess energy of 0.9 eV when OH(X) is produced. As the excitation energy of OH(A) is approximately 4 eV, additional kinetic energy of fast ions, which are only present in low-pressure plasmas, is necessary. Specifically, Gardner *et al* [88] report a threshold ion energy of 15 eV and the branching for the OH(A) production represents only 2% of the total cross-section. In contrast, the charge transfer to water from the helium dimer ion has been shown to be one of the dominant production mechanisms of OH(A) in DBD discharges in He containing trace amounts of water [106].

The quenching rates of OH(A) for different colliders are shown in table 5, together with the thermalization times for the OH(X) state. The thermalization times are estimated from LIF measurements of the rotational population distribution as a function of time after the production of OH(X) by photolysis of H_2O_2.

To illustrate the use of table 5, we provide an example. Assume OH(A) is produced in a 300 K air plasma by a production process which causes highly rotational excitation of the OH(A) state. Water is only present in a small amount and it does not influence the collisional quenching or the RET rate. The collisional quenching rate of air $R_Q = k_{Q,N_2} n_{N_2} + k_{Q,O_2} n_{O_2}$ is $1.3 \times 10^9\ s^{-1}$. The effective lifetime of the OH(A) state

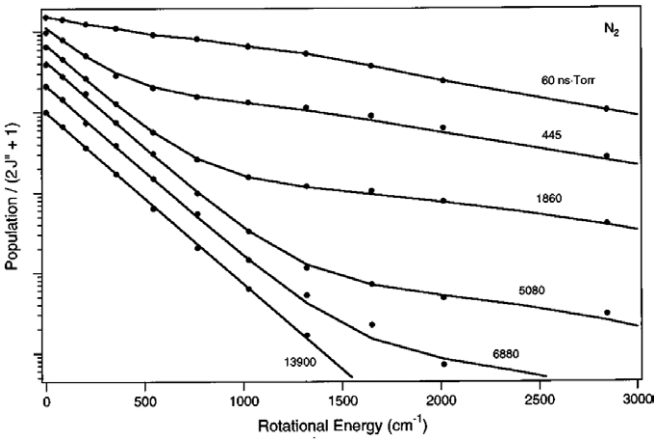

Figure 14. Boltzmann plots of OH(X) obtained by LIF at different delays after its production by photolysis of H_2O_2. The background gas is N_2 at 6.2 Torr [159]. The distributions clearly illustrate the thermalization of the nascent non-Boltzmann distribution and also the difference in thermalization time between low and high rotational levels.

$\tau_{\text{eff}} = (R_Q + \nu)^{-1}$ hence becomes 0.8 ns. In view of the 18 and 19 ns of OH(A) in N_2 and O_2, respectively, this will prohibit thermalization of the entire rotational manifold, if we assume that the thermalization time of the X and the A states are approximately the same. Nonetheless, the RET rate for the small rotational numbers is significantly faster. Considering the result in figure 14, the first four rotational levels are between 7.5 and 30 times faster thermalized than the entire rotational distribution. This leads to a thermalization time of between 0.6 and 2.4 ns which is in the range of the effective lifetime. As most of the collisional quenching rates (except for Ar and He) are similar or even faster than for air, thermalization of the OH(A) rotational levels is often strongly inhibited in molecular gases at atmospheric pressure. The reader is also referred to figure 11 for the case of atmospheric pressure water vapor. Note that the timescale for thermalization in water is smaller than in other gases, which is also in correspondence with the calculated thermalization of the OH(A) rotational distribution shown in figure 11. RET rates have been measured for different colliders and reported in the literature, see, e.g., [99, 162].

A collisional radiative model for OH(A–X) radiation in air has been developed by Levin *et al* [163]. The model

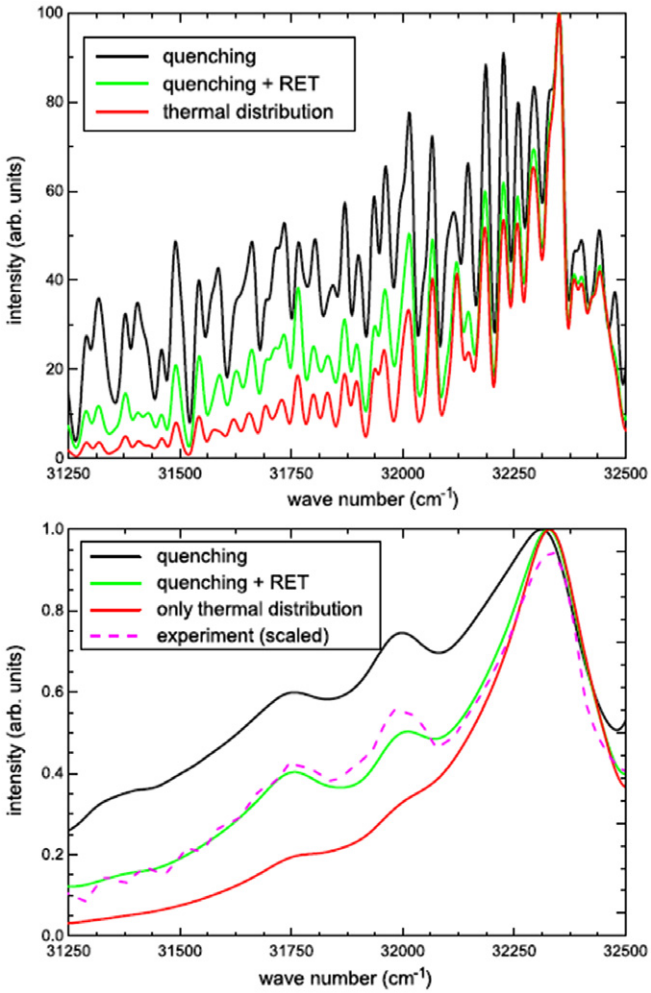

Figure 15. Simulation of OH(A–X) chemiluminescence spectra assuming formation of OH(A) with nascent distribution corresponding to a temperature parameter of 5000 K. Black: only quenching is considered. Green: Quenching and RET is taken into account. Red: emission spectrum at thermal equilibrium with $T = 2200$ K. Bottom: same spectra, convoluted with a Gaussian slit function to allow comparison with a recorded spectrum (dashed line) [164].

includes collisional quenching, pre-dissociation, spontaneous emission, RET and VET. The model assumes that neutral collision terms dominate over electron- and ion-impact processes and that collisional ionization and dissociation have negligible influence on the ro-vibrational distribution. Note that this model does not include nascent rotational distributions of OH(A) produced, for example, by electron-impact dissociation. The model is shown to be able to describe the OH(A–X) emission spectrum in a high power RF plasma torch at atmospheric pressure as well as under rarefied conditions in the bow shock of a re-entering rocket [163].

In addition, a full model including quenching, RET and a nascent non-thermal distribution which allows simulation of the chemilumiscent OH(A–X) spectra in flames was recently reported by Brockhinke *et al* [164]. An illustration of the possible large effects of RET in flames from this reference is shown in figure 15. Brockhinke *et al* reported that, under the conditions studied, the synthetic spectra do not strongly depend on the nascent rotational population distribution, which in the model is assumed to be close to a Boltzmann distribution at 5000 K. Note that in this case the non-thermal nascent distribution will be due to chemical reactions because in flames, electronic and ionic processes will not be dominant. The model is actually an extended version of the model used to produce the results presented in figure 11. In addition, the actual distribution as a function of time needs to be multiplied by the exponential decay accounting for the effective lifetime of the OH(A) and to be integrated over time. This way, the contribution to the emission originating from the different levels at different times after production is accounted for.

6.3. $N_2^+(B)$

$N_2^+(B\,^2\Sigma_u^+–X\,^2\Sigma_g^+)$ emission (first negative system of nitrogen) is often observed in air and nitrogen-containing ionizing plasmas, especially at low pressures. Due to Penning ionization, it is also a dominant emission in He even when nitrogen is only present as an impurity. The (0,0) vibrational transition is usually the strongest band and its band head is observed at 391 nm [117]. Both upper and lower electronic states are $^2\Sigma^+$ and pure case b of Hund [18]. $\Delta N = 0$ transitions are forbidden and the spectrum contains only P and R branches. In both states, due to spin-rotation interactions, each rotational level is spin-doubled with rotational numbers $J = N + 1/2$ and $J = N - 1/2$. Energy of rotational levels and the Hönl–London coefficients of the lines are given in Kovacs [16]. The spectroscopic constants of the transition can be found in [19, 20] and data for high-resolution spectroscopy has been published by Michaud *et al* [167]. An example of high-resolution spectra of the 0–0 band obtained in absorption spectroscopy and showing the spin-doubled components of the rotational lines can be found in [168].

The production mechanisms for $N_2^+(B)$ are summarized in table 6 and can differ from plasma to plasma. In low-pressure ionizing plasmas, $N_2^+(B)$ is often populated by electron-impact from the ground state of the neutral $N_2(X)$ molecule. However, when the electron temperature is not large (i.e. typically in high-density steady-state plasmas) the direct excitation from the ground state is unlikely to be dominant. A stepwise production of $N_2^+(B)$ will occur by first producing the ground state ion $N_2^+(X)$ and subsequent excitation of this ion to its excited B state. The production of the ground state ion can also occur by stepwise ionization via intermediate metastable states of N_2, or even by associative ionization [126]. Excitation of the ground state $N_2^+(X)$ ion to the $N_2^+(B)$ state is reported to occur by two main channels: direct electron-impact excitation and energy transfer in collisions with the $N_2(X)$ molecules in high vibrational levels ($\nu \geqslant 12$).

In nitrogen, high vibrational levels are populated by an effective collisional pump-up mechanism between vibrational levels. The high efficiency of this process comes from the fact that vibrational relaxation is slow and the energy gap between successive levels decreases with increasing vibrational number [169]. When two vibrationally excited $N_2(X)$ molecules collide, one of them loses a vibrational quantum which is gained by the other. This pumping process is particularly

Table 6. Production reactions for $N_2^+(B)$ and the corresponding rate coefficients. The electron excitation reactions are calculated from cross sections in the mentioned references assuming a Boltzmann distribution.

Reaction	k ($m^3\,s^{-1}$)	Remarks	Ref.
Electron excitation			
$e^- + N_2(X) \rightarrow N_2^+(B) + 2e^-$	4.9×10^{-24}–2.9×10^{-18}	$T_e = 1$–3 eV $E_{ex} = 18.75$ eV	[113]
$e^- + N_2^+(X) \rightarrow e^- + N_2^+(B)$	3.4×10^{-15}–1.9×10^{-14}	$T_e = 1$–3 eV $E_{ex} = 3.17$ eV	[165]
Vibrational states			
$N_2^+(X) + N_2(X; v \geqslant 12) \rightarrow N_2^+(B) + N_2(X; v - 12)$	7×10^{-17}		[132]
Metastable excitation			
$He(2^3S) + N_2(X) \rightarrow N_2^+(B) + He + e^-$	7×10^{-16}		[166]
Dissociative recombination			
$N_3^+ + N \rightarrow N_2^+(B) + N_2(X)$	0.2×10^{-16}		[126]

efficient in nitrogen as the vibrational transition is (optically) forbidden for homonuclear molecules and hence the relaxation time is large. As a result, the vibrational population distribution is far from a Boltzmann distribution. However, the rotational levels tend to equilibrate very quickly with the gas kinetic temperature [170]. In a 2.3 Torr glow discharge, Macko *et al* [171] have measured a rotational temperature of 500 K in the vibrational level $v = 18$ of the ground state. No strong rotational excitation is thus necessarily expected.

As the rotational constants of the $N_2(X)$, $N_2^+(X)$ and the $N_2^+(B)$ state are very similar, (2.00 cm^{-1}, 1.93 cm^{-1} and 2.08 cm^{-1}, respectively [20, 118]) electron excitation from either $N_2(X)$ or $N_2^+(X)$ will produce a similar thermalized rotational population distribution, with the restriction that the rotational distributions in these ground states are in equilibrium with the gas temperature. Therefore, the rotational population distribution of $N_2^+(B)$ excited by electron impact usually reflects the gas temperature. In reduced pressure nitrogen-containing discharges, high rotational excitation has been observed and is ascribed to the production of $N_2^+(B)$ by heavy particle collisions, namely vibrational pumping [172, 173].

Rotational distributions of $N_2^+(B)$ produced by penning ionization of $N_2(X)$ by helium metastable atoms has been reported by Richardson and Setser [58] to be very similar to those of the neutral precursor molecule. At room temperature, the rotational temperature of $N_2^+(B)$ was between 30 and 50 K larger than the gas temperature.

Bibinov *et al* [174] found significantly larger rotational temperatures of $N_2^+(B$–$X)$ compared with $N_2(C$–$B)$ emission in He DBD discharges and explained the difference by the fact that the $N_2^+(B$–$X)$ is produced in the plasma filaments but $N_2(C$–$B)$ is produced by metastable pooling in the bulk gas. The latter thus yields a smaller (average) rotational (gas) temperature. Both Ionascut–Nedelcescu *et al* [175] and Hofmann *et al* [27] found that the $N_2^+(B)$ rotational temperature in He plasmas at atmospheric pressure overestimates the gas temperature. An increase in apparent rotational temperature with increasing distance (and thus also increasing air entrainment) from the nozzle of an atmospheric pressure plasma jet operating in helium is reported in [176]. The increasing air entrainment reduces the effective lifetime of the $N_2^+(B)$ which prevents complete thermalization of the state. The high rotational excitation is attributed to the charge exchange reaction of the helium ion with the ground state $N_2(X)$ molecule [176]. In relatively pure He discharges, the production mechanisms will be Penning ionization which could also induce a moderate rotational excitation (see above).

Table 7. Quenching rates for $N_2^+(B)$ for different species.

Reaction	k ($m^3\,s^{-1}$)	Ref.
$N_2^+(B) \rightarrow N_2^+(X) + h\nu$	$1.6 \times 10^7\,s^{-1}$	[132]
N_2	8.8×10^{-16}	[178]
O_2	10.5×10^{-16}	[178]
H_2	6.8×10^{-16}	[135]
CO	1.9×10^{-16}	[135]
H_2O	8.6×10^{-16}	[135]

$N_2^+(B$–$X)$ emission with significant ro-vibrational excitation is also observed in a recombining plasma ($T_e = 0.2$ eV) without the presence of direct electron excitation. It is argued in [177] that the production is due to charge transfer of N^+ with $N_2(A)$, as is clear from overpopulation of resonant $v = 6$ and 7 levels of the $N_2(B)2\Sigma_u^+$ state.

Collisional quenching rates for $N_2^+(B)$ are shown in table 7. To the authors' knowledge only RET cross-sections of $N_2^+(X)$ in He are reported in the literature [179]. The cross-section for the total RET from levels $N = 0$ to $N = 15$ decreases from 18.8 to 11.9 $Å^2$. The value for $N = 10$ (i.e. 13.8 $Å^2$) is about 10 times larger than the RET cross-section for $OH(A; v = 0, N = 10)$ in He (see figure 9). The fact that the rotational constant is smaller leads to a slower decrease in RET with increasing rotational number and a significantly faster thermalization of the rotational states. In view of similar rotational constants for $N_2^+(B)$ and $N_2(C)$ states, a similar thermalization time is to be expected.

6.4. Short overview of often-used ro-vibrational transitions

As shown in the case of $N_2(C$–$B)$, when possible, it is advantageous to use molecules which are present in the feed gas and to avoid molecules which are produced by dissociative or associative processes. The latter almost always lead to non-thermal nascent rotational distribution. A nice illustration is the work of Andre *et al* [186] who compared the rotational

Table 8. Overview of some regularly used ro-vibrational transitions for gas temperature determination. Production mechanisms and nascent rotational distributions are mentioned when reported. See text for more details.

Transition	λ (nm)	Gas	Production mech.	Nascent rot. distr.	Ref.
$N_2(B\,^3\Pi_g–A\,^3\Sigma_u^+)\delta\nu = 3$	620–690	N_2 (air)			[24, 180]
$O_2(b\,^1\Sigma_g^+–X\,^3\Sigma_g^-)$	758–772				[3, 181]
$H_2(d\,^3\Pi–a\,^3\Sigma)$	590–620	H_2	e^- excit.		[4]
$CH(A\Delta–X\,^2\Pi)$	420–440	CH_4	e^- dissoc. excit.	≈3600–4000 K	[107]
$NH(A–X)$		NH_3	e^- dissoc. excit.	≈1700 K	[72]
$CO(B\,^1\Sigma^+–A\,^1\Pi)(0, 2)$	508–520	CO_2	e^- dissoc. excit.	—	[182]
$SiF(A\,^2\Sigma–X\,^2\Pi)$		SiF_4	e^- dissoc. excit.	high rot. excit.	[183]
$CF(B\,^2\Delta–X\,^2\Pi)$	202–205	CF_4	e^- dissoc. excit.	high rot. excit.	[184]
$NO(A\,^2\Sigma^+–X\,^2\Pi)$	240–248	N_2–O_2	$N_2(A)$ excit.	high rot. excit.	[49]
$CN(B\,^2\Sigma^+–X\,^2\Sigma^+)$	386	CH_4–N_2	—	—	[185]
$C_2(d\,^3\Pi_g–a\,^3\Pi_u)$	513–517	C_nH_m			[7]

temperatures of $N_2(C)$, $O_2(B)$, $OH(A)$ and $NO(A)$ in a glow (-like) discharge in humid air at atmospheric pressure. The rotational temperatures are 2200, 2200, 2600 and 3800 respectively. The rotational temperatures of OH and NO, which are formed in the discharge, are significantly larger than the rotational temperatures of molecules present in the gas.

Apart from the $N_2(C–B)$ transition, other transitions of nitrogen can be used just like emission bands from H_2 (e.g. Fulcher α band) and the atmospheric band of O_2 whose upper state can be produced by electron excitation. A summary of transitions regularly used in the literature is given in the table 8 and is discussed below.

Moon and Choe [3] have compared T_r of the $OH(A)$, $N_2^+(B)$ and $O_2(b)$ in an ac driven atmospheric pressure plasma in He with humid air impurities and T_r of $OH(A)$ and $O_2(b)$ in a MW induced plasma. The rotational temperatures of the plasmas were 930 K and 2200 K, respectively. The potential use of $O_2(b)$ to obtain the gas temperature is clearly shown. The example of the spectra for the MW torch is given in figure 16. It is interesting to note that the fit of the $OH(A–X)$ spectrum is not great for $\lambda > 309$ nm, which could be attributed to a non-equilibrium behavior of the rotational distribution, while the discrepancies in the case of the $O_2(b\,^1\Sigma–X\,^3\Sigma)$ can be ascribed to the overlapping argon lines. Note that Andre *et al* [186] used the Schumann–Runge transition $O_2(B\,^3\Sigma_u^-–X\,^3\Sigma_g^-)$ with similar result. At reduced pressure (0.5–5 Torr), Touzeau *et al* [181] compared the rotational temperature of the $O_2(b)$ state to the rotational temperature of the ground state and the first metastable $O_2(a\,^1\Delta)$-state, measured by anti-Stokes Raman scattering, and found excellent agreement. It is worth noting that both $O_2(b\,^1\Sigma)$ and $O_2(a\,^1\Delta)$ are metastable states with very long lifetimes and consequently the rotation–translation equilibrium is established, as in the ground-state $O_2(X)$.

Nitrogen transitions other than the $N_2(C–B)$ system can be used. Biloiu *et al* [180], for example, used the first positive system of nitrogen to obtain rotational temperatures. Earlier work is performed by Simek *et al* [187, 188]. Note that the radiative lifetime of $N_2(B)$ (a few μs) is significantly larger than the radiative lifetime of the $N_2(C)$ state (38 ns). As a consequence, the molecule spends more time in the B–state and has more collisions with the bath gas. RET is thus usually efficient in the $N_2(B)$ state to equilibrate rotation and translation temperatures. However, a drawback is that $N_2(B)$ is more subject to the collisional quenching and at atmospheric pressure, the first positive system is much weaker than the second positive system. Nonetheless the $N_2(B–A)$ emission

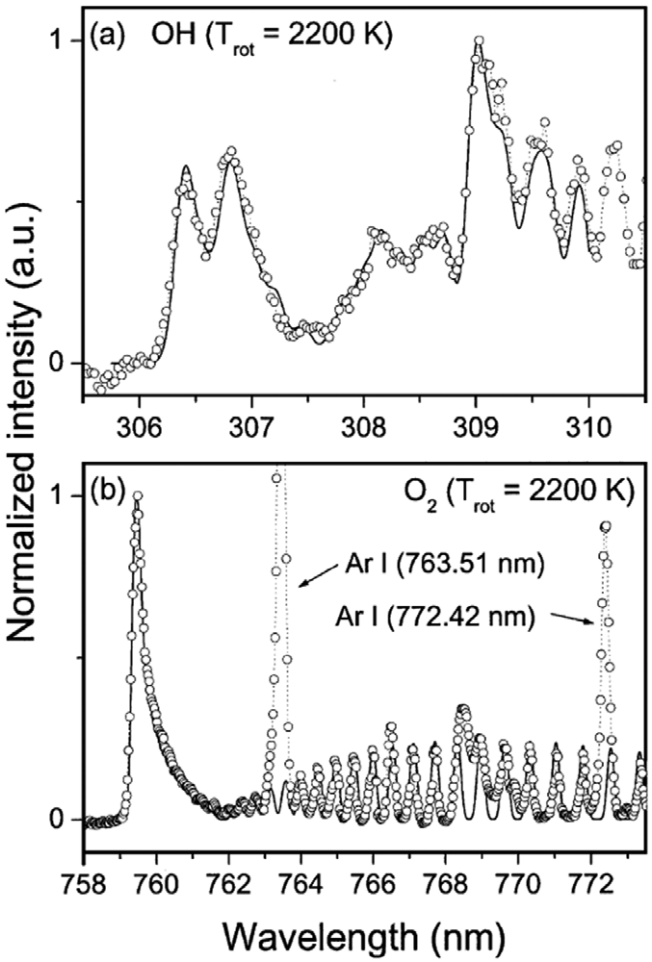

Figure 16. Rotational temperature measured from the $OH(A–X)$ and $O_2(b–X)$ transitions in an atmospheric pressure air microwave torch plasma [3].

was successfully used for gas temperature measurements in microdischarges operating in argon at hundreds of Torr [24, 189], for which the use of the $N_2(C–B)$ bands is problematic. The energy of the rotational levels of the $N_2(B)$ and $N_2(A)$ states and the Hönl–London coefficients of the rotational lines are given in Kovacs [16] and the most reliable high-resolution spectroscopic constants of the transition was published by Roux and Michaud [190]. Nonetheless, the second positive system remains by far the most used transition for gas temperature determination.

The upper state of the H_2 Fulcher α band does not have significant interaction with other excited states of hydrogen and can be easily used when it is produced by electron excitation. When the RET is fast enough, the rotational constants of the excited state can be used in the Boltzmann plot. However, in the low-pressure limit, the situation is more complicated as electron excitation can induce a significant change in rotational quantum number due to the small mass of H_2. In this case, an excitation–deactivation balance equation is necessary to obtain the rotational temperature of the ground state from the emission spectrum. For most cases, the correction of the obtained rotational temperature with the ratio of the rotational constants of the ground and excited states is given [4]. Examples are worked out in detail for the Q-branch in the PhD Thesis of De Graaf [191]. Additional references are, e.g., [192, 193]. While many researchers report that the Fulcher α band is reliable, there exist plasma conditions for which the Fulcher α band rotational temperature does not correlate to the gas temperature [194].

Many examples of molecular excited states which are similar to the case of $OH(A)$ produced in dissociation processes are reported in the literature. An illustrative example is the comparison between different rotational temperatures found for CF, CN, C_2, CO and SiF in an inductively coupled CF_4 plasma [183]. The reported rotational temperatures are 1250 K, 1600 K, 1800 K, 1800 K and 2300 K respectively. This is a clear example of non-equilibrium rotational distributions. Although the different temperatures also appear to relate to the expected spatial distributions of the molecules. The species expected to be formed near the electrode (C_2, CO, SiF) have higher temperatures than species formed in the bulk. Cruden *et al* [184] suggested that CF is created with a highly rotationally and vibrationally excited nascent distribution, which could explain its higher rotational temperatures in comparison with CO. Indeed, according to Cruden *et al*, for their reported plasma conditions, the lifetime of the CF molecule is similar to the rotational relaxation time. Nonetheless, both examples illustrate that the rotational distribution of the excited states strongly depends on the plasma conditions and thus on its production mechanism.

Another example of strong emission of CH, C_2 and CN is found downstream in the low T_e region of an expanding arc [195]. Under these conditions direct electron dissociative excitation is small and the production processes need to be recombination reactions. Similar to the above example, a significant difference in rotational temperatures is found.

The case of $CH(A)$ was investigated in detail in a DBD discharge by Luque *et al* [107]. The conclusions are identical to the $OH(A)$ system: the nascent rotational distribution is highly ro-vibrationally excited. It is suggested that dissociative electron excitation could be responsible for it but many rates of the production of $CH(A)$ from, e.g., the ground state CH are not well known. Nonetheless, at high pressures, thermalization of the rotational states with small N is possible. This should allow one to obtain the gas temperature from the $CH(A–X)$ spectra. The RET decreases significantly with increasing rotational number [101] (just as is the case for $OH(A)$ and $N_2(C)$) resulting in significantly larger time for the thermalization of the high number rotational levels. Similarly, $NH(A)$ can be produced by dissociative electron excitation [72]. There exist data on quenching and RET rates for $NH(A)$ and its rotational level lifetime dependence [109, 110] which allow estimation if the rotational temperature is a good indication of the gas temperature [196].

As shown above, CO has also been used to obtain estimates of the kinetic temperature, although it has been shown that care needs to be taken as mixing of different electronic states, which can be vibrational level dependent, can significantly disturb the rotational distribution [52]. An example of the use of the Angström system $CO(B\,^1\Sigma^+–A\,^1\Pi)$ can be found in [182].

$NO(A)$ is often formed by direct excitation rather than by dissociation processes. In $N_2–O_2$ mixtures with significant amounts of nitrogen, often energy transfer from $N_2(A)$ is responsible for the excitation of the ground state to the A-state [49, 121]. This process is found to produce an overpopulation in high rotational levels [49]. An example of a larger rotational temperature of $NO(A)$ in comparison with $N_2(C)$, even at atmospheric pressure can be found in [197]. In He–air MW jets at atmospheric pressure, van Gessel and Bruggeman found that the $NO(A)$ rotational temperature was larger than the $NO(X)$ rotational temperature [104]. This was explained by the fact that the RET rate strongly depends on the gas temperature and that the thermalization of the rotational manifold takes significantly more time at elevated temperatures [104]. In both cases $N_2(A)$ excitation is most likely responsible for the production of $NO(A)$ from $NO(X)$.

The $CN(B–X)$ system has been validated by Chu *et al* [185] by LIF (on the same transition) to yield a good estimate of the gas temperature in a $CH_4–H_2$ discharge used for the growth of diamond. The transition is included in the Lifbase database in which the necessary data and references can be found [111]. The formation process of $CN(B)$ in an atmospheric pressure DBD discharge is investigated by Dilecce *et al* [198] who concluded that recombination processes of C and N (assisted by a third body) in the afterglow and the N + CH reaction were responsible for forming the excited CN radical. The $CN(B)$ state is showing strong vibrational excitation. Rotational excitation was not investigated in this case. There exist limited amount of data on RET coefficients (at least for the ground state) to estimate rotational thermalization times [102].

Lombardi *et al* [7] showed reasonable correspondence between T_r values deduced from the Swan system ($C_2(d\,^3\Pi_g – a\,^3\Pi_u)$) by both emission and absorption spectroscopy. Absorption is possible because the lower state is a metastable state. Similar conclusions were found by Bai *et al* [199] when comparing the rotational temperature of the $C_2(d)$ state with

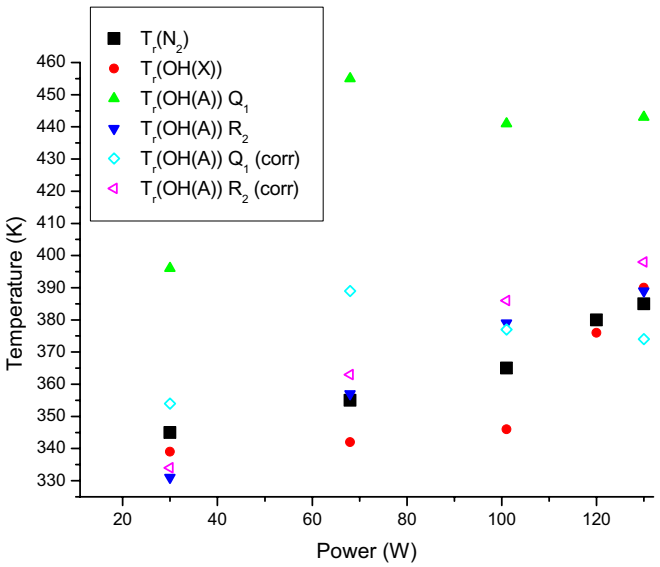

Figure 17. Rotational temperatures measured from $N_2(C–B)$ emission, absorption on $OH(X)$ and $OH(A)$ emission for different powers at a fixed water concentration of 1100 ppm in an He RF atmospheric pressure glow discharge. For the emission from the $OH(A)$ state, the values are deduced from the R_2 and Q_1 branches, and presented with and without correction for the auto-absorption in the plasma [9].

the one from the $N_2(C–B)$ emission in the same discharge. On the other hand, Meinel and Krauss [200] reported a non-Boltzmann distribution for the same Swan transition (observed in emission). In that work, it was suggested that $C_2(d\,^3\Pi_g)$ was formed by dissociative electron excitation from C_x, $x > 2$, similar to $OH(A)$ production from water.

There exist many other transitions which are reported in the literature for different plasmas used for specific applications, for example [38, 201–207]; however, a complete overview is outside the scope of this review.

7. Experimental artifacts

Up to now, we discussed chemical and physical processes which can lead to non-thermal rotational population distributions. In this section experimental artifacts, which also have a physical cause, but which are related to the way of recording the spectra are discussed.

7.1. Self-absorption

When the lower state of an observed rotational band is a highly populated ground state or a metastable state, re-absorption of the emission between the location of the emitter and the exit window of the plasma chamber can occur. The rotational levels of the ground state follow in most cases a Boltzmann distribution. Since those of them which are the most populated will reabsorb more photons from the transitions of which they are the lower state, self-absorption is a temperature-dependent process. The high rotational levels are suffering less from the self-absorption than the lower ones. This can lead, in some cases, to a significant distortion on the measured relative intensities of rotational lines, and hence on the deduced temperature of the excited state. An example of the rotational temperature of $OH(A)$ in an atmospheric pressure He–H_2O RF plasma, in which the rotational density distribution of the ground state $OH(X)$ was also obtained, is shown in figure 17. The gas temperature is well represented in this case by the rotational temperature of $N_2(C)$ and $OH(X)$. A correction for the absorption of emission lines inside the plasma, calculated from the measured $OH(X)$ densities, yields a much better correspondence of T_r from $OH(A)$ with the gas temperature [9]. Note that the correction depends on the rotational levels' densities in the ground state which is temperature dependent. As a consequence, the correction itself is gas temperature dependent!

This effect has been observed for many cases. Two additional examples are the $NO(A–X)$ transition [208] ($NO(X)$ is a ground state) and the C_2 Swan system [209] (the $C_2(a)$ state is a metastable state).

7.2. Inhomogeneities: spatial and temporal resolution

Optical emission spectroscopy is often a line of sight measurement. In dc arc discharges, researchers for years have been applying Abel inversion to obtain radially resolved emission profiles, from which the temperature profile was deduced [210, 211]. Abel inversion requires fitting and accurate line of sight measurements, which is often not possible in atmospheric pressure (filamentary) plasmas partly because of the small size and non-stationary nature of the discharge.

An example of highly spatial resolved rotational temperature measurements of $N_2(C–B)$ in an atmospheric pressure micro-glow discharge is made by Staack *et al* [212]. A variation between 800 and 1450 K is found with the maximum gas temperature in the negative glow region. Spatially averaged data are reported to correspond to this large temperature as the strongest emission of $N_2(C–B)$ is found to be in the negative glow. Bruggeman *et al* [213] have also found that in the case of an atmospheric pressure glow discharge with water cathode, the maximum emission intensity of $OH(A–X)$ is in the positive column while the $N_2(C–B)$ emission has its maximum intensity in the anode and cathode zones. Note that spatially averaged measurements would thus yield bulk temperatures for $OH(A–X)$ and anode and cathode zone temperatures for $N_2(C–B)$. In atmospheric pressure glow discharges, radially resolved emission intensities, which can vary for different species, have been obtained by Arkhipenko *et al* [214].

Spatially resolved gas temperatures have been measured by Rayleigh scattering in an atmospheric pressure glow discharge, in a plasma filament and in plasma jets [27, 32, 33, 215–217]. Results show significant gradients which can only be resolved by highly spatially resolved OES measurements (see figure 18). The presence of a strong temperature gradient can also be an issue for the line broadening measurements by absorption techniques and sometimes models are necessary to extract the spatial profiles [218].

It is also very important to consider the transient nature of a plasma. The emission intensity can change drastically between

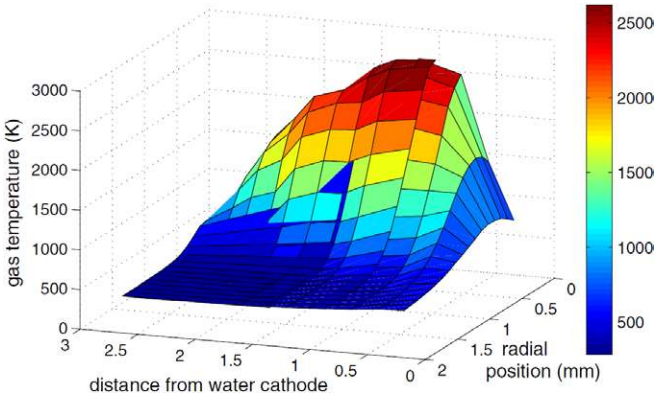

Figure 18. Spatially resolved gas temperature as obtained by Rayleigh scattering in a glow discharge in air between a pin metal anode and a water cathode in a 3 mm gap [32]. The color scale is the gas temperature in units K.

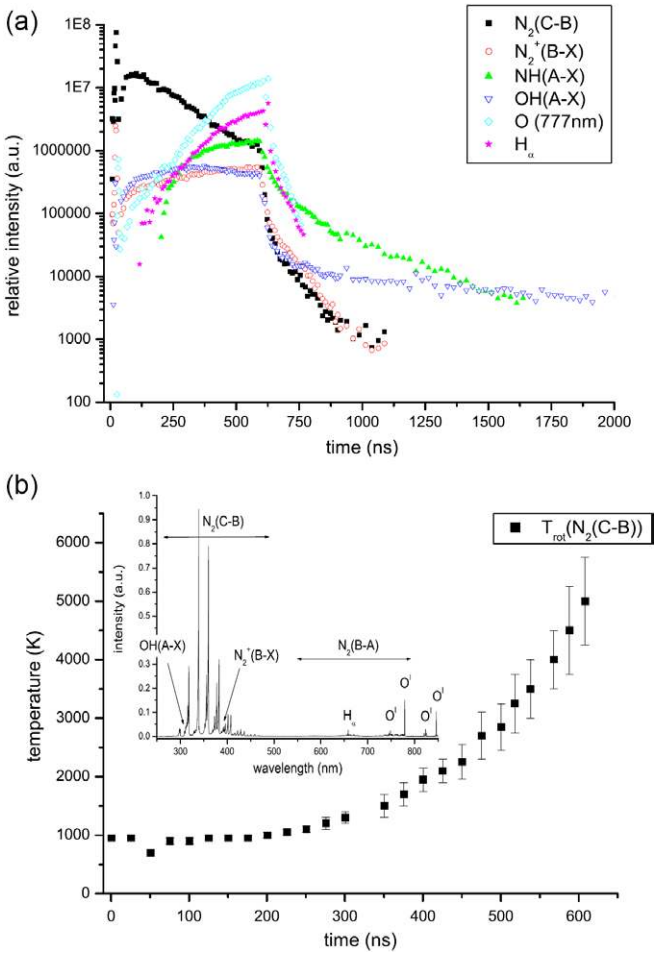

Figure 19. Relative emission intensities and gas temperature, as obtained from the rotational temperature of $N_2(C-B)$, as a function of time for a 600 ns pulsed plasma in a metal pin–water electrode geometry [219].

the ignition phase, ionizing phase and the recombination phase as is shown for a 600 ns pulsed plasma in air generated in a metal pin–water electrode geometry in figure 19. It is immediately clear that the emission of $N_2(C-B)$ initially has a maximum and decreases by an order of magnitude during the pulse. This means that if time-averaged data were considered, the gas temperature would be estimated to be close to 1000 K, while the gas temperature (as obtained by the rotational temperature of $N_2(C)$, has a maximum of about 5000 K at the end of the pulse. In addition, the NH(A–X) emission is maximum at the end of the pulse, which means that if NH(A) has a rotational temperature representative of the gas temperature, the time averaged rotational spectrum of NH(A–X) would yield a rotational temperature which could be 2000–3000 K higher than the rotational temperature of nitrogen. A striking example is given by van der Horst *et al* [215] who found that $N_2(C-B)$ was only found in the ignition phase of the discharge while during the spark phase only ionic and atomic emissions were observed. In this case the rotational temperature was close to the ambient temperature (350 K) while even between 1 to 10 μs after the discharge, the obtained gas temperatures by Rayleigh scattering were between 700 and 800 K.

The above examples are for discharges with temperatures of 1000 K or more, but differences in rotational temperatures of different excited states in close-to-room-temperature DBD discharges have also been attributed to differences in their excitation mechanisms. Bibinov *et al* [174] reported that NO(A), OH(A) and $N_2(C)$ yield rotational temperatures of 310 K (i.e. the gas temperature) independent of the investigated plasma conditions while the $N_2^+(B)$ increased from 380 K up to 550 K with increasing N_2 concentration. In helium-based plasmas, the $N_2^+(B)$ emission is produced by Penning ionization of the He metastable atoms. This process is very fast and inhibits the diffusion of He metastable atoms outside the filament. In addition, as shown above, the Penning ionization process causes only small rotational excitation, while under the present experimental conditions the effective lifetime remains above 2 ns, which should lead to a thermalized distribution within this state. The discrepancy in rotational temperatures of different molecules is thus due to the spatial inhomogeneity of their density and thus directly related to the formation process. It is estimated that both OH(A) and NO(A) are produced by excitation of their respective ground state molecules by $N_2(A)$, while $N_2(C)$ can be produced by pooling of $N_2(A)$. An analysis of the time-resolved $N_2^+(B)$ in a similar DBD discharge has also been made by a chemical and fluid-dynamic model to show that indeed the rotational temperature of $N_2^+(B)$ reflects the gas temperature in the microdischarge area [220].

In conclusion, it is thus very important to consider spatial and temporal variations in the plasma as it can significantly affect the emission intensity and also the rotational temperature. As shown by the above examples, knowledge of the formation processes of the excited states, together with temporal and spatial resolved emission profiles can significantly help one to explain potentially observed discrepancies of rotational temperatures of different excited states. Note that LIF or Rayleigh scattering are ideal techniques to obtain the gas temperature with high spatial (size of the laser beam) and temporal (a few ns laser pulse duration) resolution.

8. Spectra interpretation and analysis

In this section, the acquisition of spectra and important features of the spectrometer which needs to be considered in the spectrum analysis and fitting are summarized. Different methods to determine the rotational temperature from spectra are compared and examples of fitting routines are presented.

8.1. Detector and spectroscopic systems

Recording spectrally resolved emission spectra of the light-emitting species in plasmas is usually performed by a grating spectrometer. The light is collected by an optical fiber or imaging optics and then focused on the entrance slit of a spectrometer. In the spectrometer, the light is received by a grating which diffracts it by splitting the emitted light with different wavelengths in different spatial angles. Collected by a collimating mirror, the light is focused, forming images (at different positions for different wavelengths) on the exit plane of the spectrometer. When a charge coupled device (CCD camera) or a diode array is used for the light detection, it is located precisely at the exit plane to capture the whole image, which corresponds to the intensity distribution at different wavelengths. When a photo-multiplier tube (PMT) is used as a detector, it is placed behind a narrow slit located precisely at the exit plane. In this later case, the spectra are obtained by the rotation of the grating. An illustration of the images formed on a CCD camera of an argon micro-hollow-cathode discharge at 427.217 nm (argon line) and 427.752 nm (argon ion line) is shown in [189]. More details can be found in [221] and standard textbooks referenced therein.

8.1.1. Wavelength-dependent sensitivity of the detector. The result of the light detection is a spectrogram with intensity (or number of photons) over wavelength. However, the light distribution of the source may differ from the detected spectrogram for several reasons:

- photons get absorbed on their way from the source to the detection device (especially for (V)UV));
- the wavelength-dependent detection efficiency of the PMT or CCD;
- the wavelength-dependent spectrometer efficiency;
- the spectral sensitivity of the mirrors, collection optics, windows and fibers used.

The measured spectrogram needs to be corrected by the spectral sensitivity of the complete measurement setup in order to get the correct intensity distribution of the light source. The sensitivity calibration is performed using a light source whose wavelength distribution is known. The quotient of detected and known intensity is the spectral sensitivity. Typical sources used are, e.g., the tungsten halogen lamp (visible) and deuterium lamp (for the UV). In many cases, when the domain of interest is limited to a few nm, e.g., as a single vibrational band is recorded, the wavelength-dependent sensitivity can be neglected. This is the case provided that the measured wavelength is not on the edge of the nominal working range of all elements of the light detection system and the spectrometer.

8.1.2. Wavelength calibration and background subtraction. The wavelength calibration is performed by recording spectra of a source with known wavelengths (for instance discharge lamps containing atomic gases which have well-defined atomic emission lines). Since the dispersion/diffraction of light is non-linear, the wavelength assignment to pixel positions (for a CCD) or grating motor position (for the PMT) is non-linear. When a CCD is used, the manufacturer of the spectrometer usually provides a fit of the fourth order, but often a fit of the third order is adequate. This fit gives the wavelength assignment of all pixels of the CCD (often 1024) which means that for each pixel there is a slight deviation in the assignment between the actual and the recorded wavelength (deviation from the fit function). Thus, a new wavelength assignment may be necessary when the correct wavelength of the recorded signal is essential. This is especially the case when a high-resolution spectrum in a large wavelength range is fitted (see below).

Wavelength-dependent background subtraction is in many cases straightforward but, e.g., for high-density discharges a strong background can be present due to, e.g., Bremsstrahlung or black-body radiation. In this case, it is important to measure a broad spectrum so the background can be subtracted easily (see, for example, figure 5 in [222] for an OH spectrum with large background).

8.1.3. Apparatus and instrumental function. The spectral shape of the emission from a single atom at rest is a Lorenz profile, with the so-called natural line width. In addition, as already introduced above, Doppler, collisional and Stark broadening of lines are often significant in a plasma. However, usually the experimental setup has a significant impact on the observed line shape. Indeed, the resolution of the system (including spectrometer and detector) induces a broadening of the measured emission line which is called instrumental or apparatus function.

In the case of the PMT, the resolution is determined by the width of the entrance and exit slits, the focal length of the spectrometer and the number of grooves of the grating. In the case of the CCD, the exit slit is wide open (or not present) and the resolution is determined by the pixel size on the CCD sensor and not the exit slit.

The Voigt shape of the actual line profile must be convoluted with the apparatus function and often the resulting recorded line is much broader than its original Voigt shape, which cannot be resolved any further. For typical spectrometers with a resolution of >15 pm, FWHM, the recorded line profile of the emission from a low-pressure gas discharge lamp, for which the line width is known to be small ($\approx$1 pm FWHM), can be used to obtain in good approximation the apparatus function. For a better determination of the apparatus function, it is often possible to fit the line profile to the rotational spectrum which often contains several fully resolved rotational lines.

In the case of a small entrance slit, the recorded line shape can be approximated by a Gauss function. But for a broader slit opening, the shape is more trapezoidal. Due to an imperfect light path, the line shape can get asymmetric. In

the case of an iCCD, additional broadening can occur due to the intensifier because some neighboring pixels of the CCD are connected. The exact knowledge of the shape of a single atomic transition is essential when a multi-line spectrum needs to be simulated (as for instance a partially or non-resolved rotational spectrum). When a grating is used for diffraction of the light, the full-width at half-maximum (FWHM) of a single atomic line depends on the wavelength, (gets smaller with increasing wavelength) whereas the general shape remains largely the same. Thus, the line shape of a single atomic transition can be used to make a model of the line shape used in the spectrum of superimposed lines like a rotational spectrum. However, the 'model line' should be in the same wavelength range as the spectrum to be fitted.

8.2. Representing and fitting rotational spectra

8.2.1. Boltzmann plot. As already shown in many examples above, rotational spectra can be represented in a Boltzmann plot if fully resolved rotational lines are recorded. A logarithmic plot of the intensity reduced by the A coefficient and the degeneracy of the level against the rotational energy of the level yields a straight line when the rotational population is in equilibrium (obeying a Boltzmann distribution). The rotational temperature can be directly obtained from the slope. This approach has a major advantage when compared with fitting of partially resolved rotational spectra as deviations from a Boltzmann distribution can be easily observed. In addition, without having to make assumptions one can see the shape of the rotational population distribution (a superposition of two Boltzmann distributions or even three as in figure 1).

8.2.2. Band head ratios and widths. An often-used technique is to use band head ratios for which tables have been published to estimate the gas temperature from specific rotational bands. This technique is very easy and fast if it is applied with the proper spectral resolution (as the ratios depend on spectral resolution). Tables or figures have been published for, e.g., OH(A–X) [1, 222].

Widths of bands have also been used to estimate the rotational temperature from the $N_2(C–B)$ [1] and $N_2(B–A)$ [188] transitions. Inherently, this technique can be prone to error as it assumes a Boltzmann distribution and the validity of this assumption cannot be checked with this method. It is thus always good practice to check if a thermal distribution is present, especially in the case of OH.

8.2.3. Synthetic spectra calculation and fitting algorithms. When a spectrum needs to be fitted, a synthetic spectrum needs to be constructed and convoluted with the instrumental function of the spectra recording device. While the line shape due to the instrumental function is considered in the fitting, the correction of the spectral sensitivity, and wavelength calibration is normally performed before setting up the fitting routine.

Several approaches include a manual fitting of the spectra. The most straightforward approach is to create a synthetic spectrum considering the known parameters of the line positions, Hönl–London coefficients and rotational energies of all the lines. This spectrum can be convoluted with the instrumental function and only one fitting parameter, i.e. the rotational temperature is used (when a Boltzmann distribution of the rotational levels is assumed) to obtain correspondence with the experimental spectrum.

The determination of the rotational temperature by fitting is an iterative process. It can be performed by a least-squares fitting using a simplex downhill algorithm. Van Gessel *et al* [124] used standard fitting routines in Matlab. A theoretical spectrum is computed and compared with the measured and corrected spectrum. Next, the fitting parameters are varied until a best accordance is reached. In order to use automatic fitting programs for the shape of rotational spectra, the measured data must have been corrected for the spectral sensitivity. In addition, a very good accordance (small fitting error) between measured and theoretical spectra can only be reached by a correct wavelength assignment of the intensities. As stated above, the wavelength calibration by the spectrometer manufacturer may not be sufficient and a small mismatch of the line positions can lead to a large error of the fitted spectrum shape. If the spectrum is spread over a larger range than a few nm, then even the small decrease in the line width with increasing wavelength needs to be considered (sometimes) in order to obtain an excellent correspondence between the experimental and synthetic spectrum. In summary, a full fledge fitting software does not only provide the variation of T_r but also the dependence of the line width on the wavelength and the wavelength assignment of the pixel positions of the CCD. Collisional quenching and pre-dissociation of rotational levels can of course also be included in the software as fitting parameters.

Even under consideration of the above-mentioned corrections to the experimental spectrum, there are many cases that the rotational spectrum cannot be fitted very well (sometimes not at all) with a Boltzmann distribution of the rotational populations as seen in many examples above. Often, this can be solved by a fitting with contributions of two groups of molecules to the spectra with two different Boltzmann temperatures. In this case, three fitting parameters have to be determined: the ratio of the amount of molecules in each group and two rotational temperatures.

An example of fitting a non-thermal ro-vibrational spectrum of OH(A–X) (0,0) and (1,1) is shown in figure 20. Note that the single temperature fit does not yield a good fit at all. The assumption of two different Boltzmann rotational distributions in vibrational levels 0 and 1 yields a much better fit. Despite the initial wavelength calibration of the spectra, a fit including wavelength alignment of features in the experimental and simulated spectra leads to a significant improvement. This is clearly illustrated by the fact that $T_2^{(1,1)}$ is a much more realistic value when the wavelength alignment is made. Note that the neglecting of the wavelength alignment causes an error of at least 10 K in the fit, without even considering other sources of errors. To illustrate the quality of the fit, the experienced reader will even notice that the vibrational bands (1–0) and (2–1) of the $N_2(C–B)$ at 315.9 and 313.6 nm are visible in

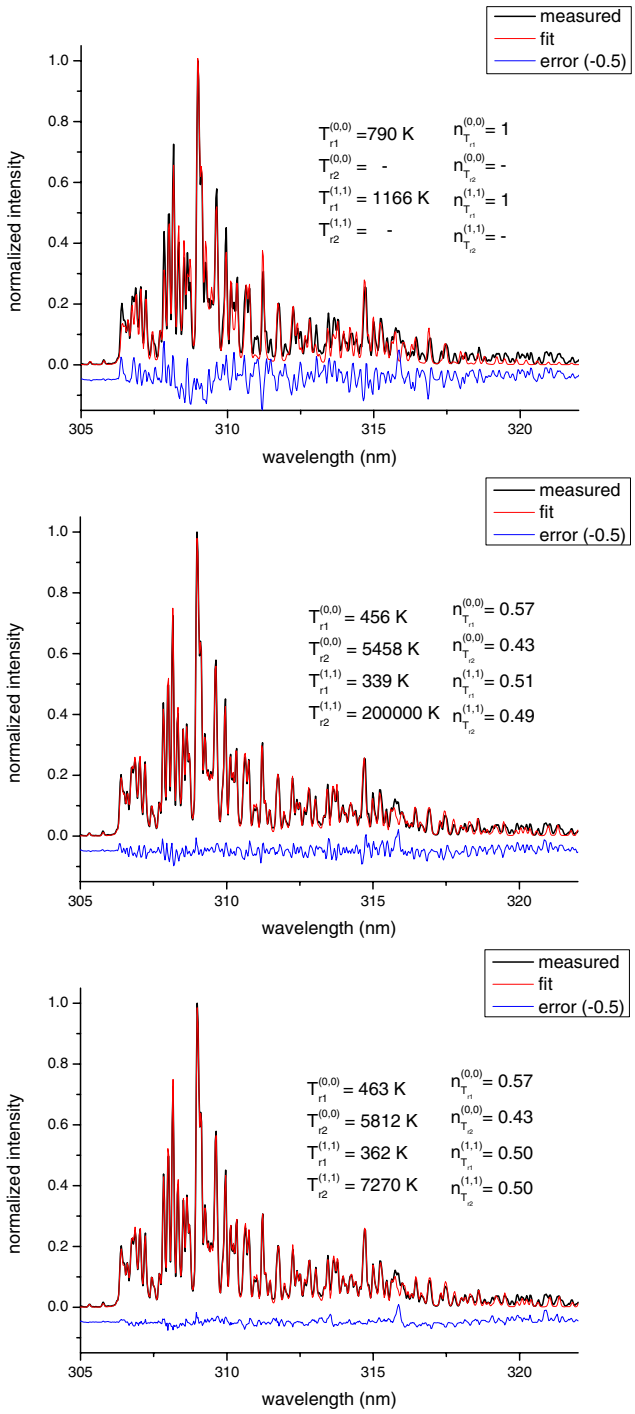

Figure 20. Fitting of an OH(A–X) emission spectrum obtained by time-resolved emission (at 590 ns) during a nanosecond pulsed discharge in a helium bubble. Details of the plasma can be found in [223]. The figures show fitting results assuming a Boltzmann rotational distribution for vibrational level 0 and 1 (upper figure) assuming a superposition of two Boltzmann rotational distributions for vibrational level 0 and 1 (middle figure) and additionally including a fit of the wavelength alignment (lower figure), respectively. The spectrum is recorded with a resolution of 0.076 nm FWHM and the measured line profile of a low-pressure Hg lamp is used as apparatus function.

the residue of the fit. Note that the band head ratio method (which is not applicable for non-Boltzmann distributions) from the tables published in [222] yields rotational temperatures of 1000–1200 K which are exceeding the gas temperature by almost a factor of 3.

There exist(ed) open source programs such as Lifbase [111] and Specair [224] to manually fit spectra. Specair only considers thermal rotational distributions in air plasmas and Lifbase allows one to include non-thermal distributions by user-defined rotational population distributions. Many research groups have their own code for spectral fitting.

8.2.4. Collisional radiative model. All of the above approaches assume that the nascent rotational population distribution is not determining the observed rotational spectra, or can at least be captured using a superposition of 2 or more Boltzmann distributions.

When the nascent rotational population distribution strongly determines the rotational spectrum, the best approach is of course to make a full collisional radiative model of the production of the excited state, the collisional processes and the fluorescence involved, for every rotational level. Although this approach has been made for LIF (e.g. the Laskin software [225] developed at the university of Bielefeld), this is rather rare for plasma processes (see the two examples described in the OH(A) section). This approach requires detailed knowledge of the production processes and also the nascent rotational distribution, which is often not known on a rotational level scale in non-equilibrium plasmas.

8.3. Influence of spectral resolution

Rotational temperatures can be obtained from moderately resolved spectra of, e.g., OH(A–X) and $N_2(C$–$B)$. See, e.g., Yu *et al* [226], Bruggeman *et al* [130] and Machala *et al* [227], which used resolutions between 0.2 and 0.6 nm FWHM. Note that these spectral resolutions can be obtained with on the shelf pre-configured fiber optic spectrometers which make the technique available and easy to use for non-spectroscopy experts. However, since in this particular case individual rotational structures are not resolved, detailed knowledge is necessary concerning the following points:

- self-absorption;
- production mechanisms of excited states and nascent rotational distribution;
- overlapping rotational bands;
- apparatus function.

It needs to be stressed that many non-thermal distributions can be approximated by a Boltzmann distribution, especially for low-resolution spectra. It is thus very important to know if non-thermal behavior is to be expected when only low-resolution spectra are acquired. Similarly, while overlapping bands are easily detected at high resolution, more care needs to be taken for low-resolution spectra. An example of a $N_2^+(B)$ spectrum with a moderate resolution of 0.05 nm is shown in figure 21. It clearly illustrates the necessity of accurate fits for partially resolved rotational spectra. Note the small deviation for the single temperature fit, while a two-temperature fit yields a rotational temperature of 200 K lower [59].

A variation of 10% in the slit function for $N_2(C$–$B)$ at 0.45 nm FWHM leads to a change in the rotational

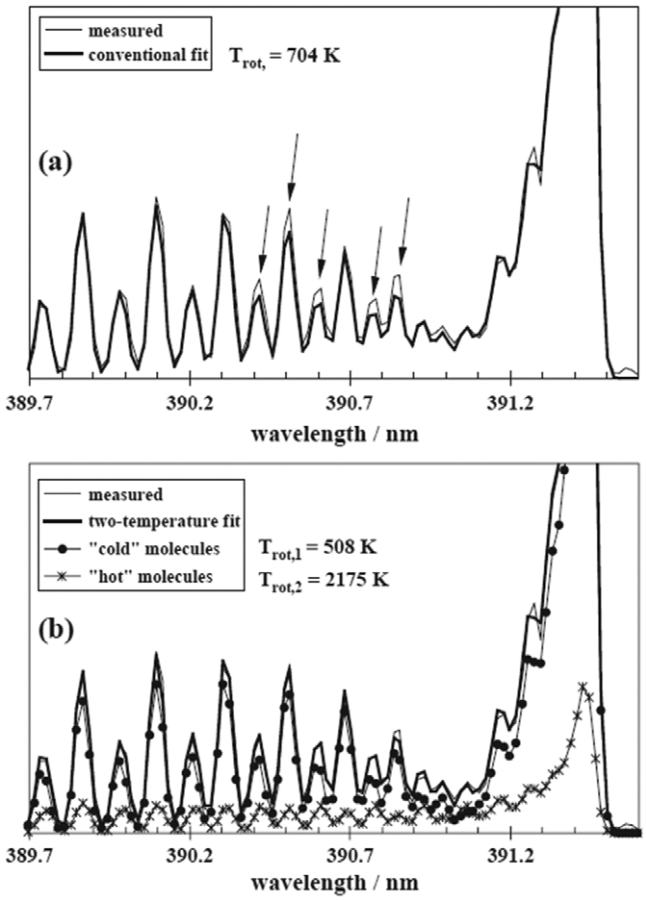

Figure 21. Fitting of the $N_2^+(B–X)$ (0–0) band obtained with a spectral resolution of 0.05 nm with a conventional Boltzmann distribution and a superposition of two temperatures [59].

temperature of 50 K for a Boltzmann temperature of 350 K spectrum. For moderately resolved spectra, the accuracy on the rotational temperature is thus strongly determined by the apparatus function. When using high-resolution spectra, (a few pm FWHM) accuracies in the rotational temperature of about 10 K are possible (see, e.g., [9].) In the latter case, the line profile can be fitted to the spectrum, as resolved rotational lines (at least for higher rotational numbers) can be observed in many cases. This significantly enhances the accuracy.

8.4. Absolute emission and absorption

In order to be able to estimate production mechanisms of the excited states (which determine the nascent distribution) it is beneficial to obtain time-resolved emission (in time modulated plasmas) and to have data on absolute emission intensities and absorption. From the absolute emission intensity one can determine the amount of excited species produced to which possible production mechanisms can be attributed, at least if the rate coefficients (and plasma parameters on which it depends) are known. Absorption data yield rotational distributions of the ground state molecule which are in most cases in thermal equilibrium. Their rotational temperature is representative of the gas temperature. In addition, it allows one to estimate ground state density or radicals such as OH, which enable estimation of the effect of direct electron excitation to the upper states, if the cross-sections of the reaction are known.

9. Conclusions

This review paper provides the necessary background to answer one question: for which conditions are the rotational levels of an excited state, from which the emission is observed, in translational–rotational equilibrium? The different processes which can influence the rotational population distribution have been summarized and several examples have been given. Some technical details on recording spectra and determining rotational temperatures from spectra are also given.

Before using rotational spectra to estimate the gas temperature, it is always good practice to try to estimate the effective lifetime of the excited state and compare it with the rotational thermalization time. Three cases, based on the ratio between the effective lifetime τ_{eff} and the time necessary for thermalization of the rotational manifold $\tau_{thermal}$, can be discerned,

- $\tau_{eff} \gg \tau_{thermal}$: the rotational distribution is a Boltzmann distribution with the rotational temperature equal to the gas temperature,
- $\tau_{eff} \ll \tau_{thermal}$: the rotational distribution is an image of the formation process and not directly related to the gas temperature. Only in the case when electron excitation from the ground state is dominant, a mapping of the ground state rotational distribution into the rotational levels of the excited state occurs and the gas temperature can be directly determined,
- $\tau_{eff} \approx \tau_{thermal}$: the rotational distribution is determined by thermalizing collisions and the formation process. In many cases a superposition of two Boltzmann distributions can be used to fit the rotational spectrum. The lower rotational states are sometimes partly thermalized and a temperature can be obtained from their density distribution.

Note that in several cases, rotational thermalization times are not very accurately known and it is advantageous if the production mechanism of the excited state is known in order to assess if the nascent rotational distribution favors the high rotational levels. If no data exist, a good estimate is to calculate the elastic collision frequency of the molecule with the bath gas and consider that about ten collisions are necessary for the thermalization.

As is often stated incorrectly, the high collisionality in atmospheric pressure plasmas is not *a priori* a guarantee for the thermalized rotational distributions, as the collisional quenching of the excited state can significantly reduce the effective lifetime. We would like to stress that no general recommendations on gas temperature determination can be given and thus case by case needs to be investigated. It is good practice to always use two different excited states (when available) to check if the rotational temperatures are equal, or one can use two independent methods to measure the gas temperature.

To fully grasp molecular spectra, collisional radiative models need to be constructed. This is a way which is almost unexplored in complex molecular plasmas. These models would not only allow one to get information on the excited state densities, the production processes and the gas temperature but potentially may yield information about other plasma parameters including, e.g., electron temperatures and ground state radical densities. Nonetheless, in many cases such models only exist for specific molecules such as N_2 up to very high vibrational levels, but without modeling the rotational distributions. In many cases, reaction cross-sections are missing or are not known accurately enough to predict rotational distributions. This lack illustrates the usefulness of representing rotational distributions with (a superposition of) Boltzmann distributions which allows one to obtain qualitative and often even quantitative data on the gas temperature.

Acknowledgments

PJB would like to thank Bram van Gessel for providing his numerical code for the calculation of RET coefficients and LIF spectra. The code has been adapted to obtain the results in figure 11. Sampson Moore is acknowledged for his valuable suggestions. VL likes to thank Jorge Luque for numerous discussions on OH spectra. Finally all authors would like to express their gratitude to all authors and publishers for permission to reproduce figures from their works.

References

[1] Laux C, Spence T, Kruger C and Zare R 2003 *Plasma Sources Sci. Technol.* **12** 125–38
[2] Ishii I and Montaser A 1991 *Spectrochim. Acta* B **46** 1197–206
[3] Moon S and Choe W 2003 *Spectrochim. Acta* B **58** 249–57
[4] Astashkevich S, Kaning M, Kaning E, Kokina N, Lavrov B, Ohl A and Ropcke J 1996 *J. Quant. Spectrosc. Radiat. Transfer* **56** 725–51
[5] Bruggeman P, Schram D, Gonzalez M A, Rego R, Kong M G and Leys C 2009 *Plasma Sources Sci. Technol.* **18** 025017
[6] Bruggeman P and Brandenburg R 2013 *J. Phys. D: Appl. Phys.* **46** 464001
[7] Lombardi G, Benedic F, Mohasseb F, Hassouni K and Gicquel A 2004 *Plasma Sources Sci. Technol.* **13** 375–86
[8] Ramos R, Cunge G, Touzeau M and Sadeghi N 2008 *J. Phys. D: Appl. Phys.* **41** 115205
[9] Bruggeman P, Cunge G and Sadeghi N 2012 *Plasma Sources Sci. Technol.* **21** 035019
[10] Kohsehoinghaus K 1994 *Prog. Energy Combust. Sci.* **20** 203–79
[11] Lang T, Motzkus M, Frey H and Beaud P 2001 *J. Chem. Phys.* **115** 5418–26
[12] Drake M and Rosenblatt G 1978 *Combust. Flame* **33** 179–96
[13] Montello A, Yin Z, Burnette D, Adamovich I and Lempert W 2013 *J. Phys. D: Appl. Phys.* **46** 464002
[14] Daily J 1997 *Prog. Energy Combust. Sci.* **23** 133–99
[15] Verreycken T, van der Horst R M, Baede A H F M, Van Veldhuizen E M and Bruggeman P J 2012 *J. Phys. D: Appl. Phys.* **45** 045205
[16] Kovacs I 1969 *Rotational Structure in the Spectra of Diatomic Molecules* (Bristol: Institute of Physics Publishing)
[17] Kuznetsova L 2012 *The Data Bank on Radiative and Energy Parameters for Diatomic Molecules* (Chemical Department, Moscow State University www.elch.chem.msu.ru/raden/index.htm)
[18] Herzberg G 1950 *Molecular Spectra and Molecular Structure: Spectra of Diatomic Molecules* (Princeton, NJ: van Nostrand Reinhold)
[19] 2012 Nist: http://webbook.nist.gov/chemistry/
[20] Huber K P and Herzberg G 1979 *Molecular Spectra and Molecular Structure: Constants of Diatomic Molecules vol IV* (New York: van Nostrand-Reinhold)
[21] Gigosos M and Cardenoso V 1996 *J. Phys. B: At. Mol. Opt. Phys.* **29** 4795–838
[22] Konjevic N 1999 *Phys. Rep. Rev. Sect. Phys. Lett.* **316** 339–401
[23] Griem H R 1964 *Plasma Spectroscopy* (New York: McGraw-Hill)
[24] Belostotskiy S G, Ouk T, Donnelly V M, Economou D J and Sadeghi N 2010 *J. Appl. Phys.* **107** 053305
[25] Hubner S, Sadeghi N, Carbone E A D and van der Mullen J J A M 2013 *J. Appl. Phys.* **113** 143306
[26] Yubero C, Dimitrijevic M S, Garcia M C and Calzada M D 2007 *Spectrochim. Acta* B **62** 169–76
[27] Hofmann S, van Gessel A F H, Verreycken T and Bruggeman P 2011 *Plasma Sources Sci. Technol.* **20** 065010
[28] Booth J, Derouard J, Fadlallah M and Sadeghi N 1993 *J. Appl. Phys.* **74** 862–7
[29] Wang Q, Koleva I, Donnelly V and Economou D 2005 *J. Phys. D: Appl. Phys.* **38** 1690–7
[30] Belostotskiy S G, Donnelly V M, Economou D J and Sadeghi N 2009 *IEEE Trans. Plasma Sci.* **37** 852–8
[31] Miles R, Lempert W and Forkey J 2001 *Meas. Sci. Technol.* **12** R33–51
[32] Verreycken T, van Gessel A F H, Pageau A and Bruggeman P 2011 *Plasma Sources Sci. Technol.* **20** 024002
[33] van Gessel A F H, Carbone E A D, Bruggeman P J and van der Mullen J J A M 2012 *Plasma Sources Sci. Technol.* **21** 015003
[34] Wertheimer M R, Ahlawat M, Saoudi B and Kashyap R 2012 *Appl. Phys. Lett.* **100** 201112
[35] Kersten H, Rohde D, Berndt J, Deutsch H and Hippler R 2000 *Thin Solid Films* **377** 585–91
[36] Farley D R 2010 *J. Chem. Phys.* **133** 094303
[37] Lavrov B, Ostrovsky V and Ustimov V 1979 *Zh. Eksp.—Alnoi Teor. Fiz.* **76** 1521–9
[38] Osiac M, Lavrov B and Ropcke J 2002 *J. Quant. Spectrosc. Radiat. Transfer* **74** 471–91
[39] Gans T, Schulz-von der Gathen V and Dobele H 2001 *Plasma Sources Sci. Technol.* **10** 17–23
[40] Stepowski D and Cottereau M 1981 *J. Chem. Phys.* **74** 6674–9
[41] Setser D, Stedman D and Coxon J 1970 *J. Chem. Phys.* **53** 1004–20
[42] Nguyen T and Sadeghi N 1983 *Chem. Phys.* **79** 41–55
[43] Xu L, Sadeghi N, Donnelly V M and Economou D J 2007 *J. Appl. Phys.* **101** 013304
[44] Nguyen T, Sadeghi N and Pebaypey J 1974 *Chem. Phys. Lett.* **29** 242–6
[45] Sadeghi N and Setser D 1981 *Chem. Phys. Lett.* **82** 44–50
[46] Krumpelmann T and Ottinger C 1987 *Chem. Phys. Lett.* **140** 142–7
[47] Ottinger C, Vilesov A and Xu D 1995 *Chem. Phys.* **192** 49–64
[48] Bachmann R, Ehlich R, Ottinger C, Rox T and Sadeghi N 2002 *J. Phys. Chem.* A **106** 8328–38
[49] DeBenedictis S, Dilecce G and Simek M 1997 *J. Phys. D: Appl. Phys.* **30** 2887–94
[50] Vanvliembergen E, Vredenbergt E, Kaashoek G, Jaspar J, Vanlanen M, Janssens M, Verheyen M and Beijerinck H 1987 *Chem. Phys.* **114** 117–36

[51] Sadeghi N, Colomb I, Stoyanova J, Setser D and Zhong D 1995 *J. Chem. Phys.* **102** 2744–59
[52] Zikratov G, Setser D and Sadeghi N 2000 *J. Chem. Phys.* **112** 10845–57
[53] Endoh M, Tsuji M and Nishimura Y 1983 *J. Chem. Phys.* **79** 5368–75
[54] Lin G, Maier J and Leone S 1986 *J. Chem. Phys.* **84** 2180–6
[55] Lin G, Maier J and Leone S 1986 *Chem. Phys. Lett.* **125** 557–60
[56] Lin G, Maier J and Leone S 1985 *J. Chem. Phys.* **82** 5527–35
[57] Huwel L, Guyer D, Lin G and Leone S 1984 *J. Chem. Phys.* **81** 3520–35
[58] Richards W and Setser D 1973 *J. Chem. Phys.* **58** 1809–25
[59] Linss V 2005 *Spectrochim. Acta* B **60** 253–63
[60] Herbst E and van Dishoeck E 2009 *Annu. Rev.: Astron. Astrophys.* **47** 427–80
[61] Schinke R 1993 *Photodissociation Dynamics: Spectroscopy and Fragmentation of Small Polyatomic Molecules* (Cambridge: Cambridge University Press)
[62] Schinke R 1985 *Chem. Phys. Lett.* **120** 129–34
[63] Engel V, Staemmler V, Vanderwal R, Crim F, Sension R, Hudson B, Andresen P, Hennig S, Weide K and Schinke R 1992 *J. Phys. Chem.* **96** 3201–13
[64] Weide K and Schinke R 1987 *J. Chem. Phys.* **87** 4627–33
[65] Gericke K, Klee S, Comes F and Dixon R 1986 *J. Chem. Phys.* **85** 4463–79
[66] Hradil V, Suzuki T, Hewitt S, Houston P and Whitaker B 1993 *J. Chem. Phys.* **99** 4455–63
[67] Lin S, Lin S, Lee Y, Chou Y, Chen I and Lee Y 2001 *J. Chem. Phys.* **114** 7396–406
[68] Butenhoff T, Carleton K and Moore C 1990 *J. Chem. Phys.* **92** 377–93
[69] Spiglanin T and Chandler D 1987 *J. Chem. Phys.* **87** 1577–81
[70] Mohlmann G, Beenakker C and Deheer F 1976 *Chem. Phys.* **13** 375–85
[71] Beenakker C, Deheer F, Krop H and Mohlmann G 1974 *Chem. Phys.* **6** 445–54
[72] Tokue I and Iwai M 1980 *Chem. Phys.* **52** 47–53
[73] Beenakker C, Verbeek P, Mohlmann G and Heer F 1975 *J. Quant. Spectrosc. Radiat. Transfer* **15** 333–40
[74] Mumma M, Stone E and Zipf E 1975 *J. Geophys. Res.* **80** 161–7
[75] Sonnenfroh D, Caledonia G and Lurie J 1993 *J. Chem. Phys.* **98** 2872–81
[76] Shibagaki K, Asakawa R, Hayashi D and Sasaki K 2008 *Plasma Fusion Res.: Rapid Commun.* **3** 005
[77] Tsuji M, Nakamura M, Nishimura Y and Obase H 1995 *J. Chem. Phys.* **103** 1413–21
[78] Tsuji M, Nakamura M, Nishimura Y and Obase H 1998 *J. Chem. Phys.* **108** 8031–8
[79] Cossart-Magos C and Cossart D 2000 *J. Chem. Phys.* **112** 2148–54
[80] McElroy D, Walsh C, Markwick A, Cordiner M, Smith K and Millar T 2002 *The UMIST Data Base for Astrochemistry 2012*
[81] Tielens A 2010 *The Physics and Chemistry of Interstellar Medium* (Cambridge: Cambridge University Press)
[82] Oka T 2012 *Phil. Trans.* A **370** 4991–5000
[83] Green S 1975 *Astrophys. J.* **201** 366–72
[84] Matejka M, Ocadlik S, Jasik J, Martisovits V and Veis P 2002 *ESCAMPIG (Grenoble, France)* **16** 277–8
[85] Tabayashi K and Shobatake K 1988 *J. Chem. Phys.* **88** 835–44
[86] Kanda K, Ito H, Someda K, Suzuki K, Kondow T and Kuchitsu K 1989 *J. Phys. Chem.* **93** 6020–4
[87] Tsuji M and Nishimura Y 1990 *Kyushu University Institutional Repository: The Reports of Institute of Advanced Material Study* vol 4 pp 163–74
[88] Gardner J, Dressler R, Salter R and Murad E 1992 *J. Chem. Phys.* **97** 2473–80
[89] Tanaka N, Takayanagi M and Hanazaki I 1996 *Chem. Phys. Lett.* **254** 40–6
[90] Park M J, Kang K W and Choi J H 2012 *Chem. Phys. Chem.* **13** 1289–96
[91] Park J, Lee H, Kwon H, Kim H, Choi Y and Choi J 2002 *J. Chem. Phys.* **117** 2017–29
[92] Umemoto H, Asai T and Kimura Y 1997 *J. Chem. Phys.* **106** 4985–91
[93] Pomerantz A, Ausfelder F, Zare R, Althorpe S, Aoiz F, Banares L and Castillo J 2004 *J. Chem. Phys.* **120** 3244–54
[94] Chang Y P, Hsiao M K, Liu D K and Lin K C 2008 *J. Chem. Phys.* **128** 234309
[95] Chikan V and Leone S 2005 *J. Phys. Chem.* A **109** 10646–53
[96] Creighan S, Perry J and Price S 2006 *J. Chem. Phys.* **124** 114701
[97] Schroter L, David R and Zacharias H 1991 *Surf. Sci.* **258** 259–68
[98] Gadzuk J, Landman U, Kuster E, Cleveland C and Barnett R 1982 *Phys. Rev. Lett.* **49** 426–30
[99] Kienle R, Lee M and KohseHoinghaus K 1996 *Appl. Phys.* B **63** 403–18
[100] Wang Q, Doll F, Donnelly V M, Economou D J, Sadeghi N and Franz G F 2007 *J. Phys. D: Appl. Phys.* **40** 4202–11
[101] Cooper J and Whitehead J 1993 *J. Chem. Soc.—Faraday Trans.* **89** 1287–90
[102] Fei R, Lambert H, Carrington T, Filseth S, Sadowski C and Dugan C 1994 *J. Chem. Phys.* **100** 1190–201
[103] Lee S, Luque J, Reppel J, Brown A and Crosley D 2004 *J. Chem. Phys.* **121** 1373–82
[104] van Gessel A and Bruggeman P 2013 *J. Chem. Phys.* **138** 204306
[105] Bruggeman P, Iza F, Guns P, Lauwers D, Kong M G, Aranda Gonzalvo Y, Leys C and Schram D C 2010 *Plasma Sources Sci. Technol.* **19** 015016
[106] Ricard A, Decomps P and Massines F 1999 *Surf. Coat. Technol.* **112** 1–4
[107] Luque J, Kraus M, Wokaun A, Haffner K, Kogelschatz U and Eliasson B 2003 *J. Appl. Phys.* **93** 4432–8
[108] Copeland R, Dyer M and Crosley D 1985 *J. Chem. Phys.* **82** 4022–32
[109] Smith W, Brzozowski J and Erman P 1976 *J. Chem. Phys.* **64** 4628–33
[110] Yarkony D 1992 *J. Chem. Phys.* **97** 1838–49
[111] Luque J and Crosley D 1999 *SRI International Report MP 99-009*
[112] Bacri J and Medani A 1982 *Physica* B and C **112** 101–18
[113] Itikawa Y 2006 *J. Phys. Chem. Ref. Data* **35** 31–53
[114] Piper L 1988 *J. Chem. Phys.* **88** 231–9
[115] Sadeghi N, Cheaib M and Setser D 1989 *J. Chem. Phys.* **90** 219–31
[116] Cao Y and Johnsen R 1991 *J. Chem. Phys.* **95** 7356–9
[117] Pearse R W B and Gaydon A G 1963 *The Identification of Molecular Spectra* (London: Chapman and Hall)
[118] Laher R and Gilmore F 1991 *J. Phys. Chem. Ref. Data* **20** 685–712
[119] Roux F, Michaud F and Vervloet M 1993 *J. Mol. Spectrosc.* **158** 270–7
[120] Debenedictis S and Dilecce G 1995 *Chem. Phys.* **192** 149–62
[121] Simek M, Babicky V, Clupek M, DeBenedictis S, Dilecce G and Sunka P 1998 *J. Phys. D: Appl. Phys.* **31** 2591–602
[122] Isola L, Lopez M and Gomez B J 2011 *J. Phys. D: Appl. Phys.* **44** 375204
[123] Velazco J, Kolts J and Setser D 1978 *J. Chem. Phys.* **69** 4357–73
[124] van Gessel A F H, Hrycak B, Jasinski M, Mizeraczyk J, van der Mullen J J A M and Bruggeman P J 2012 *J. Instrum.* **7** C02054

[125] van Gessel A F H, Hrycak B, Jasinski M, Mizeraczyk J, van der Mullen J J A M and Bruggeman P J 2013 *J. Phys. D: Appl. Phys.* **46** 095201
[126] Akishev Y, Grushin M, Karalnik V, Petryakov A and Trushkin N 2010 *J. Phys. D: Appl. Phys.* **43** 215202
[127] Knewstubb P and Tickner A 1962 *J. Chem. Phys.* **37** 2941–9
[128] Davis G and Gottscho R 1983 *J. Appl. Phys.* **54** 3080–6
[129] Donnelly V and Malyshev M 2000 *Appl. Phys. Lett.* **77** 2467–9
[130] Bruggeman P, Schram D C, Kong M G and Leys C 2009 *Plasma Proces. Polym.* **6** 751–62
[131] Ropcke J and Ohl A 1994 *Contrib. Plasma Phys.* **34** 575–86
[132] Guerra V, Sa P and Loureiro J 2004 *Eur. Phys. J.—Appl. Phys.* **28** 125–52
[133] Dilecce G, Ambrico P F and De BenedictiS S 2007 *Chem. Phys. Lett.* **444** 39–43
[134] Pancheshnyi S, Starikovskaia S and Starikovskii A 2000 *Chem. Phys.* **262** 349–57
[135] Pancheshnyi S, Starikovskaia S and Starikovskii A 1998 *Chem. Phys. Lett.* **294** 523–7
[136] Raud J, Laan M and Jogi I 2011 *J. Phys. D: Appl. Phys.* **44** 345201
[137] Belikov A, Burshtein A, Dolgushev S, Storozhev A, Strekalov M, Sukhinin G and Sharafutdinov R 1989 *Chem. Phys.* **139** 239–59
[138] Kistemaker P and Vries A 1975 *Chem. Phys.* **7** 371–82
[139] Sharafutdinov R, Belikov A, Strekalov M and Storozhev A 1996 *Chem. Phys.* **207** 193–201
[140] Abad L, Bermejo D, Herrero V, Santos J and Tanarro I 1997 *J. Phys. Chem.* A **101** 9276–85
[141] Jain P 1980 *J. Phys. D: Appl. Phys.* **13** 25–8
[142] Billing G and Wang L 1992 *J. Phys. Chem.* **96** 2572–5
[143] Dieke G and Crosswhite H 1962 *J. Quant. Spectrosc. Radiat. Transfer* **2** 97–199
[144] Chidsey I and Crosley D 1980 *J. Quant. Spectrosc. Radiat. Transfer* **23** 187–99
[145] Riahi R, Teulet P, Ben Lakhdar Z and Gleizes A 2006 *Eur. Phys. J.* D **40** 223–30
[146] Itikawa Y and Mason N 2005 *J. Phys. Chem. Ref. Data* **34** 1–22
[147] Rowe B, Vallee F, Queffelec J, Gomet J and Morlais M 1988 *J. Chem. Phys.* **88** 845–50
[148] Millar T J, Farquhar P and Willacy K 1997 *Astron. Astrophys. Suppl. Ser.* **121** 139–85
[149] Dilecce G, Simek M and De Benedictis S 2001 *J. Phys. D: Appl. Phys.* **34** 1799–806
[150] Novicki S and Krenos J 1988 *J. Chem. Phys.* **89** 7031–3
[151] Bruggeman P and Schram D C 2010 *Plasma Sources Sci. Technol.* **19** 045025
[152] Binns W and Ahl J 1978 *J. Chem. Phys.* **68** 538–46
[153] Dutuit O, Tabchefouhaile A, Nenner I, Frohlich H and Guyon P 1985 *J. Chem. Phys.* **83** 584–96
[154] Vejby-Christensen L, Andersen L, Heber O, Kella D, Pedersen H, Schmidt H and Zajfman D 1997 *Astrophys. J.* **483** 531–40
[155] Neau A *et al* 2000 *J. Chem. Phys.* **113** 1762–70
[156] Ojekull J *et al* 2008 *J. Chem. Phys.* **128** 044311
[157] German K 1975 *J. Chem. Phys.* **62** 2584–7
[158] Williams L and Crosley D 1996 *J. Chem. Phys.* **104** 6507–14
[159] Kliner D and Farrow R 1999 *J. Chem. Phys.* **110** 412–22
[160] Tamura M, Berg P, Harrington J, Luque J, Jeffries J, Smith G and Crosley D 1998 *Combust. Flame* **114** 502–14
[161] Dilecce G and De Benedictis S 2011 *Plasma Phys. Control. Fusion* **53** 124006
[162] Lengel R and Crosley D 1977 *J. Chem. Phys.* **67** 2085–101
[163] Levin D, Laux C and Kruger C 1999 *J. Quant. Spectrosc. Radiat. Transfer* **61** 377–92
[164] Brockhinke A, Krueger J, Heusing M and Letzgus M 2012 *Appl. Phys.* B **107** 539–49
[165] Crandall D, Kauppila W, Phaneuf R, Taylor P and Dunn G 1974 *Phys. Rev.* A **9** 2545–51
[166] Pouvesle J, Khacef A, Stevefelt J, Jahani H, Gylys V and Collins C 1988 *J. Chem. Phys.* **88** 3061–71
[167] Michaud F, Roux F, Davis S, Nguyen A and Laux C 2000 *J. Mol. Spectrosc.* **203** 1–8
[168] Gherman T, Eslami E, Romanini D, Kassi S, Vial J and Sadeghi N 2004 *J. Phys. D: Appl. Phys.* **37** 2408–15
[169] Massabieaux B, Gousset G, Lefebvre M and Pealat M 1987 *J. Phys.* **48** 1939–49
[170] Goyette A, Peck J, Matsuda Y, Anderson L and Lawler J 1998 *J. Phys. D: Appl. Phys.* **31** 1556–64
[171] Macko P, Cunge G and Sadeghi N 2001 *J. Phys. D: Appl. Phys.* **34** 1807–11
[172] Linss V, Kupfer H, Peter S and Richter F 2004 *J. Phys. D: Appl. Phys.* **37** 1935–44
[173] Linss V, Kupfer H, Peter S and Richter F 2005 *Surf. Coat. Technol.* **200** 1696–701
[174] Bibinov N, Fateev A and Wiesemann K 2001 *J. Phys. D: Appl. Phys.* **34** 1819–26
[175] Ionascut-Nedelcescu A, Carlone C, Kogelschatz U, Gravelle D V and Boulos M I 2008 *J. Appl. Phys.* **103** 063305
[176] Chan G C Y, Shelley J T, Wiley J S, Engelhard C, Jackson A U, Cooks R G and Hieftje G M 2011 *Anal. Chem.* **83** 3675–86
[177] Brussaard G, Aldea E, van de Sanden M, Dinescu G and Schram D 1998 *Chem. Phys. Lett.* **290** 379–84
[178] Dilecce G, Ambrico P F and De Benedictis S 2010 *J. Phys. D: Appl. Phys.* **43** 195201
[179] Plain A and Jolly J 1987 *Chem. Phys. Lett.* **135** 46–50
[180] Biloiu C, Sun X, Harvey Z and Scime E 2006 *Rev. Sci. Instrum.* **77** 10F117
[181] Touzeau M, Vialle M, Zellagui A, Gousset G, Lefebvre M and Pealat M 1991 *J. Phys. D: Appl. Phys.* **24** 41–7
[182] Drake D J, Popovic S and Vuskovic L 2009 *J. Appl. Phys.* **106** 083305
[183] Cruden B, Rao M, Sharma S and Meyyappan M 2002 *J. Appl. Phys.* **91** 8955–64
[184] Cruden B, Rao M, Sharma S and Meyyappan M 2002 *Appl. Phys. Lett.* **81** 990–2
[185] Chu H, Denhartog E, Lefkow A, Jacobs J, Anderson L, Lagally M and Lawler J 1991 *Phys. Rev.* A **44** 3796–803
[186] Andre P, Barinov Y A, Faure G and Shkol'nik S M 2011 *J. Phys. D: Appl. Phys.* **44** 375203
[187] Simek M, Dilecce G and Debenedictis S 1995 *Plasma Chem. Plasma Process.* **15** 427–49
[188] Simek M and Debenedictis S 1995 *Plasma Chem. Plasma Process.* **15** 451–63
[189] Lazzaroni C, Chabert P, Rousseau A and Sadeghi N 2010 *J. Phys. D: Appl. Phys.* **43** 124008
[190] Roux F and Michaud F 1983 *J. Mol. Spectrosc.* **97** 253
[191] de Graaf M J 1994 A new hydrogen particle source *PhD-Thesis* Eindhoven University of Technology
[192] Ropcke J, Kaning M and Lavrov B 1998 *J. Physique IV* **8** 207–16
[193] Lavrov B and Otorbaev D 1978 *Opt. Spektrosk.* **45** 1074–9
[194] Goyette A, Jameson W, Anderson L and Lawler J 1996 *J. Phys. D: Appl. Phys.* **29** 1197–201
[195] Beulens J, Gastineau C, Guerrassimov N, Koulidiati J and Schram D 1994 *Plasma Chem. Plasma Process.* **14** 15–42
[196] Hofzumahaus A and Stuhl F 1985 *J. Chem. Phys.* **82** 3152–9
[197] Staack D, Farouk B, Gutsol A and Fridman A 2006 *Plasma Sources Sci. Technol.* **15** 818–27
[198] Dilecce G, Ambrico P F, Scarduelli G, Tosi P and De Benedictis S 2009 *Plasma Sources Sci. Technol.* **18** 015010
[199] Bai B, Sawin H and Cruden B 2006 *J. Appl. Phys.* **99** 013308

[200] Meinel H and Krauss L 1969 *J. Quant. Spectrosc. Radiat. Transfer* **9** 443–50
[201] Briefi S and Fantz U 2011 *J. Phys. D: Appl. Phys.* **44** 155202
[202] Ruszczak M, Strojecki M, Lukomski M and Koperski J 2008 *J. Phys. B: At. Mol. Opt. Phys.* **41** 245101
[203] O'Brien L C, Borchert B A, Farquhar A, Shaji S, O'Brien J J and Field R W 2008 *J. Mol. Spectrosc.* **252** 136–42
[204] Zhang S, Zhen J, Zhang Q and Chen Y 2008 *J. Mol. Spectrosc.* **252** 77–80
[205] Setzer K, Borkowska-Burnecka J, Zyrnicki W, Pravilov A, Fink E, Das K, Liebermann H, Alekseyev A and Buenker R 2003 *J. Mol. Spectrosc.* **217** 127–41
[206] Setzer K D, Borkowska-Burnecka J, Zyrnicki W and Fink E H 2008 *J. Mol. Spectrosc.* **252** 176–84
[207] Brown J M and Mueller H S P 2009 *J. Mol. Spectrosc.* **255** 68–71
[208] Zhai X, Ding Y, Peng Z and Luo R 2012 *Appl. Opt.* **51** 4605–11
[209] Lange H, Huczko A and Byszewski P 1996 *Spectrosc. Lett.* **29** 1215–28
[210] Cremers C and Birkebak R 1966 *Appl. Opt.* **5** 1057–64
[211] Galley P, Glick M and Hieftje G 1993 *Spectrochim. Acta* B **48** 769–88
[212] Staack D, Farouk B, Gutsol A F and Fridman A 2007 *IEEE Trans. Plasma Sci.* **35** 1448–55
[213] Bruggeman P, Liu J, Degroote J, Kong M G, Vierendeels J and Leys C 2008 *J. Phys. D: Appl. Phys.* **41** 215201
[214] Arkhipenko V I, Kirillov A A, Safronau Y A, Simonchik L V and Zgirouski S M 2009 *Plasma Sources Sci. Technol.* **18** 045013
[215] van der Horst R M, Verreycken T, van Veldhuizen E M and Bruggeman P J 2012 *J. Phys. D: Appl. Phys.* **45** 345201
[216] van Gessel A F H, Alards K M J and Bruggeman P J 2013 *J. Phys. D: Appl. Phys.* **46** 265202
[217] Zhang S, van Gaens W, van Gessel B, Hofmann S, van Veldhuizen E, Bogaerts A and Bruggeman P 2013 *J. Phys. D: Appl. Phys.* **46** 205202
[218] Bol'shakov A, Cruden B and Sharma S 2004 *Plasma Sources Sci. Technol.* **13** 691–700
[219] Bruggeman P, Walsh J L, Schram D C, Leys C and Kong M G 2009 *Plasma Sources Sci. Technol.* **18** 045023
[220] Bibinov N, Fateev A and Wiesemann K 2001 *Plasma Sources Sci. Technol.* **10** 579–88
[221] Fantz U 2006 *Plasma Sources Sci. Technol.* **15** S137–47
[222] de Izarra C 2000 *J. Phys. D: Appl. Phys.* **33** 1697–704
[223] Bruggeman P, Verreycken T, Gonzalez M A, Walsh J L, Kong M G, Leys C and Schram D C 2010 *J. Phys. D: Appl. Phys.* **43** 124005
[224] Laux C 2002 *Physico-Chemical Modeling of High Enthalpy and Plasma Flows (von Karman Institute Lecture Series 2002–07)* ed D Fletcher *et al* (Rhode-Saint-Genése, Belgium) www.specair-radiation.net
[225] Rahmann U, Bulter A, Lenhard U, Dusing R, Markus D, Brockhumke A andKohse-Hoinghaus K 2012 *University of Bielefeld, Chemistry Department, Physical Chemistry*
[226] Yu L, Laux C, Packan D and Kruger C 2002 *J. Appl. Phys.* **91** 2678–86
[227] Machala Z, Janda M, Hensel K, Jedlovsky I, Lestinska L, Foltin V, Martisovits V and Morvova M 2007 *J. Mol. Spectrosc.* **243** 194–201
[228] Engeln R, Letourneur K G Y, Boogarts M G H, van de Sanden M C M and Schram D C 1999 *Chem. Phys. Lett.* **310** 405–410
[229] Gabriel O, van den Dungen J J A, Schram D C and Engeln R 2010 *J. Chem. Phys.* **132** 104305